ESTIMATION OF SHORTWAVE BROADBAND IRRADIANCE AT THE BOTTOM OF THE ATMOSPHERE OVER ILORIN IN CENTRAL NIGERIA USING RADIATIVE TRANSFER MODEL

A Thesis Submitted to the

Department of Space Physics

INSTITUTE OF SPACE SCIENCE AND ENGINEERING

An Affiliate of

AFRICAN UNIVERSITY OF SCIENCE AND TECHNOLOGY

In Partial Fulfilment of the Requirements for the Degree of

MASTER OF SCIENCE

By

DAUDA KASHIM AUDU

(Reg, No. 40837)

Institute of Space Science Engineering

www.isse.edu.ng

National Space Research and Agency,
Airport Road, Abuja, Nigeria

African University of and Science and Technology

www.aust.edu.ng

P.M.B. 681, Garki, Abuja Development
F.C.T, Nigeria.

SEPTEMBER 2021

CERTIFICATION

This is to certify that the thesis titled **ESTIMATION OF SHORTWAVE BROADBAND IRRADIANCE AT THE BOTTOM OF THE ATMOSPHERE OVER ILORIN IN CENTRAL NIGERIA USING RADIATIVE TRANSFER MODEL**, submitted to the school of postgraduate studies, African University of Science and Technology (AUST), Abuja, Nigeria for the award of a Master's degree, is a record of an original research carried out by **DAUDA KASHIM AUDU** in the **SPACE PHYSICS DEPARTMENT** of the Institute of Space Science and Engineering (ISSE), an affiliate of AUST.

DAUDA KASHIM AUDU		19th November 2021
Name	**Sign**	**Date**

ESTIMATION OF SHORTWAVE BROADBAND IRRADIANCE AT THE BOTTOM OF THE ATMOSPHERE OVER ILORIN IN CENTRAL NIGERIA USING RADIATIVE TRANSFER MODEL

BY

A THESIS APPROVED BY THE DEPARTMENT OF SPACE PHYSICS

RECOMMENDED: _____ 19th November 2021
Supervisor: Prof. Rabiu Babatunde Date

_____ 19th November 2021
Co-Supervisor: Dr. Olawole B. Abiye Date

Approved: _____ 19th November 2021
Head of Department: Date

DEDICATION

This thesis work is dedicated to Almighty Allah for giving me the fortitude, knowledge, perseverance and good health to pursue this degree. This is also dedicated to my parents, Alhaji Kashim Audu and Hajia Aisha N'achallu Audu, and my sister Mrs. Hauwa Sani, who have put in their best efforts to ensure I have become who I am today.

ACKNOWLEDGMENTS

I am grateful to Almighty Allah for giving me good health and seeing me through the length of the MSc program. My sincere gratitude and high appreciation to my supervisors, Professor Babatunde Rabiu and Dr. Olawale Abiye for their guidance and valuable contributions towards the success of this study.

Special heartfelt appreciation to my mentor and coach, Prof. Babatunde Rabiu for his patience, encouragement, continuous support, practical advice and guidance that have helped me complete this programme successfully. I appreciate Dr. Daniel Okoh and the staff of Space Environment Research Laboratory of Center for Atmospheric Research (SERL-CAR) for their hospitality and support during my study. My sincere appreciate goes to Mrs. Aderonke Obafaye for all her guidance during my thesis to make my work easier. I am very grateful for all the extra support that my good friend, Mr. Ephrem Tesfaye provided during my project.

I express my sincere appreciation to the Institute of Space Science and Engineering (ISSE) and African University of Science and Technology (AUST) for the scholarship to pursue this M.Sc. program and providing me with immense experience.

I am also grateful to my class mates and friends who have been of tremendous help during the course of my MSc Programme.

I would like to acknowledge the Department of Physics, University of Ilorin, where the AERONET equipment vital to this work was hosted by Professor Clement Olufemi Akoshile during the period of study.

I greatly appreciate my employer, National Space Research and Development Agency, for granting me the appropriate permission, scholarships and much needed support to pursue this MSc. program.

Special appreciation to my parents, Alhaji Kashim Audu and Hajia Aisha N'achallu Audu; and my sister Mrs. Hauwa Sani and husband Barrister Usman Sani, for their inexhaustible motivation and encouragement. I can't forget my niece, Farida Iman Sani, for encouraging and helping me rediscover my childhood enthusiasm.

God bless you all.

TABLE OF CONTENT

LIST OF FIGURES

LIST OF TABLES

ABSTRACT

Shortwave Broadband Irradiance (SBI) makes up about 96% of the Total Solar Irradiance (TSI) received on earth, and it is known to be the major driver of climate change. The SBI also contains ultraviolet radiation, which is harmful to inhabitants of Earth. The Direct Normal Irradiance (DNI) and Global Horizontal Irradiance (GHI) received at the surface in Ilorin (8.484°N, 4.675°E), Central Nigeria, have been computed using a radiative transfer model: the Simple Model of the Atmospheric Radiative Transfer of Sunshine (SMARTS). The spectral range of the study was from 280 to 4000 nm under cloudless conditions, using aerosol retrieval data from Ilorin AERONET station for the year 2020. The results were compared to the satellite based dataset of the Copernicus Atmosphere Monitoring Service (CAMS) McClear Clear-Sky Irradiation service, and showed good correlation for both sources of irradiance for the period of study. The results show that the RMSEs were comparatively low for most of the year, except during the dry season when the RMSE for the Direct Normal Irradiance (DNI) reached 171.77 W/m^2. This implies that the Copernicus Atmosphere Monitoring Service (CAMS) McClear Clear-Sky Irradiation service data is fairly accurate for estimating the irradiance values during the wet and dry seasons in Nigeria, but not for Direct Normal Irradiance (DNI) during the dry season.

CHAPTER ONE
INTRODUCTION

1.1 Background to the study

The primary energy source in the solar system radiating in all directions through the heliosphere is the Sun. This energy uin the form of electromagnetic radiation originates from the core of the Sun where nuclear fusion reactions take place. These thermonuclear reactions in its core are primarily from the proton-proton (ionized hydrogen) fusion process which requires a density of 150g/cm3 & a temperature of 15 million Kelvin (Dendy et al., 2007). The Sun gives off electromagnetic radiation over a wide range of wavelengths at varying intensities. The electromagnetic solar radiation that reaches the upper edge of the atmosphere is called extraterrestrial radiation, and the mean integral for the complete spectrum is 1,367 W/m², this is called the Solar Constant (Ångström, 1922; Darula et al., 2005).

The spectrum of solar electromagnetic radiation covers electromagnetic waves with frequencies ranging from below one hertz to above 1025 hertz, these wavelengths are from a fraction of the size of an atomic nucleus up to thousands of kilometers (Gueymard, 2009). These frequencies are grouped into separate bands of various names; beginning at the high-frequency (short wavelength) end of the spectrum they are Gamma rays, X-rays, Ultraviolet (UV), visible light, infrared, microwaves, and radio waves at the low frequency (long wavelength) end (ChemViews, 2015). These electromagnetic waves differ in characteristics, modes of production, and interact differently with matter. Gamma rays, X-rays, and high ultraviolet are classified as ionizing radiation as their photons have enough energy to ionize atoms, causing chemical reactions (Sage, 2012).

The incoming solar radiation is the primary source of energy for the Earth-atmosphere system affects the atmospheric conditions which in turn affects meteorology. The radiative equilibrium is affected by the variation of any part of the system, which can lead to changes in atmospheric circulation and temperature of the system (García et al., 2012). One of the key reasons for changes in the energy balance of the Earth-atmosphere system other than Green House Gases (GHGs), is atmospheric aerosols of natural and anthropogenic sources (Anton, 2008). They modify the energy balance in the atmosphere directly through the absorption and dispersion of solar radiation and, indirectly, by acting as nuclei of cloud condensation (Small et al., 2011), and modifying their properties such as albedo, reflectivity, and lifetime (Ghan et al., 2013; Lohmann and Feichter, 2005). The Solar constant of approximately 1361 W/m2 reaches the top of the Earth's atmosphere and attenuates as it passes through layers of the atmosphere, as a result of absorption and reflection which leads to an increase in temperature as absorbed radiation is converted to thermal energy (Coddington et al., 2016).

The spectral range significant to meteorology extends from about 200nm to 4000nm (short-wave radiation). About 96% of the extraterrestrial radiation is found in this range of the spectrum. At 500nm, the maximum radiation intensity of the solar spectrum occurs, towards the blue end of the visible range (Kawamoto and Hayasaka, 2008). Shortwave radiation is radiant energy

produced by the sun with wavelengths ranging from infrared through visible to ultraviolet. It is therefore exclusively associated with daylight hours for a particular location on the Earth's surface (Borak and Turner, 1996). Some of the incident radiation is reflected at the top of the atmosphere and clouds reflect some of those reaching lower altitudes. Also a part of the incoming radiation is absorbed by the atmosphere and some are absorbed by clouds. The albedo is the fraction of radiation reaching the surface that is then reflected into the atmosphere. The residual radiation that was neither reflected nor absorbed drives hydrologic processes such as evapotranspiration (Vuilleumier et al., 2014).

1.2 Problem Statement

The attenuation of solar irradiance by atmospheric aerosols plays a significant role in the Earth's surface energy balance and its subsequent cooling or heating effect, typically known as aerosol radiative forcing. Estimates of Surface Solar Irradiance are often used to understand the contribution of aerosols to climatic change over a given region. However, the methodology requires wavelength-dependent characterization of aerosol microphysical and optical properties through the use of a highly expensive automated Sun photometer.

1.3 Aim of the study

This work aims to estimate shortwave broadband irradiance in regions without a Sun photometer

1.4 Specific Objectives of the Study

This work intends to achieve the following objectives;

Estimate the hourly average Global horizontal and Direct normal Irradiance using the Simple Model of the Atmospheric Radiative Transfer of Sunshine (SMARTS) model; and

Validate the modeled broadband irradiance estimates against the CAMS McClear database.

1.5 Scope of the Study

This work utilized Direct Sun measurement and Aerosol inversion products from the AERONET (AErosol RObotic NETwork) station at the National Air Quality Research Laboratory, Department of Physics, University of Ilorin, situated in Ilorin, Kwara State, Nigeria (8.484°N, 4.675°E, 400m). Irradiance data from the Copernicus Atmosphere Monitoring Service (CAMS) McClear Clear-Sky Irradiation service was also used in this study. The NASRDA Centre for Atmospheric Research provides support for the activities of the National Air Quality Research Laboratory at the Department of Physics, University of Ilorin.

The spectral range of the study was from 280 to 4000 nm under cloudless conditions. The data used in this work spanned for one year (2020), and the Radiative transfer model used in the study was the Simple Model of the Atmospheric Radiative Transfer of Sunshine (SMARTS).

1.6 Limitation of the Study

Due to the COVID-19 pandemic lockdown in place, data gaps were prevalent between June and September 2020 resulting in just 26% of data available. Only a total of 32 days was available from 122 days in these four months.

1.7 Significance of the Study

The results of the present study on completion will provide an integrated approach of using satellite-based dataset and irradiance estimates from a radiative transfer model as a proxy for determining the shortwave broadband irradiance over a region without a Sun photometer.

CHAPTER TWO

LITERATURE REVIEW

2.1 Theoretical Background

The Sun is one of our solar system's most potent energy sources, sustaining life on Earth. It primarily emits electromagnetic (EM) radiation as a source of energy. The entire spectrum differs from an idealized black-body spectrum since it is made up of multiple components. At EUV and X-ray wavelengths, the Sun's atmospheric layers overlaying the visible disk-the photosphere, chromosphere, and corona (see Figure 2.1) make a significant contribution to the spectrum.

Because these layers are made up of a tenuous completely charged plasma, they can't be treated like a black body. Transient events such as micro and nano-flares, shock waves, erupting prominences, flares, and coronal mass ejections (CMEs) create short-term spikes in EUV, X-ray, gamma-ray, and radio-wave emissions because the magnetic structure of the Sun's photosphere modulates continuously (Wielicki et al., 1998)

Solar activity has been declining over the previous few decades, necessitating a re-evaluation of space weather studies. The physical processes involved in coping with diverse space weather parameters have been a challenge to scientists, with the potential to have a significant impact on modern society and humanity.

On Earth, only at the visible wavelengths and part of the radio wavelength regime-the atmosphere is fully transparent to the Sun's radiation so that solar observations at X-ray and EUV wavelengths have to be achieved through space missions. The Yohkoh mission launched on August 31, 1991, can be regarded as a milestone in terms of continuous high spatial resolution, full-disk solar remote-sensing observations at X-ray wavelengths. Until the end of its mission life-time-on December 14, 2001. It provided stunning new views of the Sun's X-ray corona (Pace et al., 2006).

Although the Sun's total irradiance Solar Constant, being roughly 1367 Wm^{-2} as measured at the distance of the Earth, varies only at the order of 0.1% in the course of the solar cycle (Froehlich, 2003). Variations at the UV- and EUV-wavelengths may have important ramifications on the Earth's atmosphere, and is a focus of atmospheric studies.

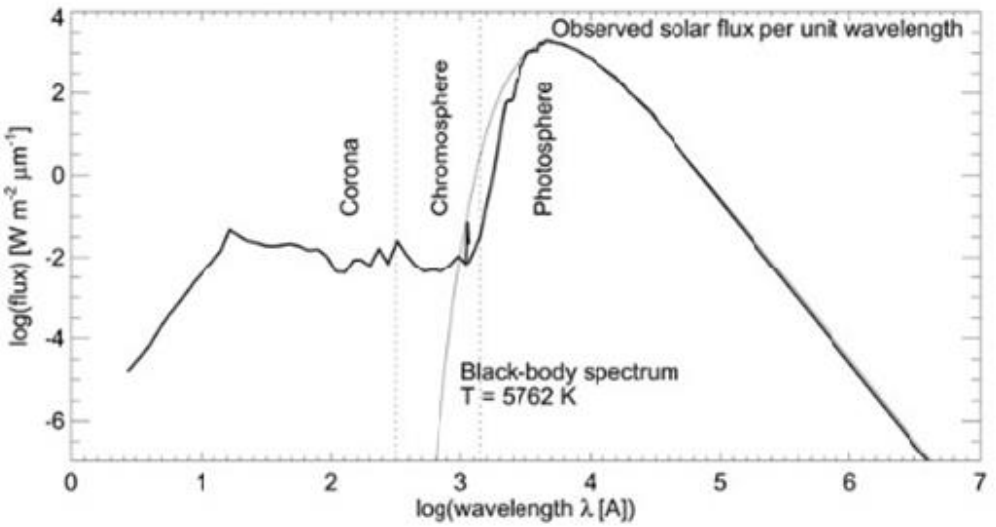

Figure 2.1*: Measured spectrum of the solar-flux as a function of wavelength in a black body with T = 5762 (Aschwanden, 2011)*

The relationship of the Sun and the Earth provides the basic framework for atmospheric physics, as a result of the radiant energy emanating from the solar surface towards the Earth's atmosphere. All of the radiant energy originating from the Sun reaches the Earth as solar radiation, consisting a vast collection of energy called the electromagnetic radiation spectrum. This includes visible light, ultraviolet light, infrared, radio waves, X-rays, and gamma rays (Wielicki et al., 1996; Wielicki et al., 1998). According to (Blanc et al., 2014) and (Gueymard, 2005), the Sun's apparent position is determined by its zenith angle and its azimuth. The algorithm determines these angles as a function of declination and hour angle. It has been shown that to have an accuracy better than 0.01° (for declination) which is more than sufficient in practical applications.

(Gueymard and Ruiz-Arias, 2015) asserts that this solar radiant energy received at the Earth's surface is of primary importance in a variety of research and application fields. The fields of application include agriculture, climate studies, atmospheric physics, remote sensing and biophysical impacts of atmospheric pollution. At varying wavelengths, biological, chemical, and physical processes are activated more easily. Nevertheless, spectral direct-beam measurements are rather rare worldwide, so the use of models on filling this gap over extended areas (Blanc et al.,

2014; Gueymard, 2012). The solar radiant energy is attenuated by tropospheric aerosols that play an important role in the Earth's climate (Pace et al., 2006; Yan, 2015), modify its vertical distribution, and affect the infrared balance, and indirectly influence the cloud structure and properties (Tolento and Robinson, 2019).

Due to the vastness of the aerosol sources, the long-range transport, and the influence of the prevailing meteorological conditions, the aerosols are difficult to be distinguished by a single aerosol type. To overcome these difficulties at a global scale, the climate prediction models and the satellite algorithms use some standard aerosol models (models with varying absorption capacity) in order to achieve the best fit between modeled and satellite irradiances in different locations in the world(Pinker et al., 1995). Thus, the aerosol models have great applicability in predicting climate change through aerosol radiative forcing and the prediction of solar radiation reaching the ground from the Sun (Kaskaoutis and Kambezidis, 2008a, 2008b).

2.2 The Sun

The Sun is a star that contains more than 99% of the total mass of the solar system, it is about 4.5×109 years in age, and has a mass of about 1.99×1030 Kg which is 333,000 times Earth's mass. The surface temperature is about 5785 K hot, and its escape velocity at the surface is 618 Km/s. The Sun is the massive ball of hot gas held together and compressed under its own gravitational attraction and thermonuclear reaction force inside (Hydrostatic Equilibrium). And its chemical compositions are Hydrogen 92.1%, Helium 7.8%, and 0.1% consists of 90 naturally occurring elements (Woolfson, 2000).

The diameter of 1.4 million km (Aschwanden, 2011), radiates electromagnetic energy from gamma-ray to radio wavelengths and also frequencies similar to that of a black body at 5770 K (Lean, 2001). The density within the sun rapidly falls with increasing distance from the core. The central density is about 150 gcm−3 and at the surface, it is about 10−7gcm−3 (Bolonkin and Friedlander, 2013). The Sun's volume can be divided into its interior and the outer solar atmosphere.

2.2.1 Solar Structure

There are three fundamental parts to the Sun's interior (which has a radius of 7.4 × 105 km) (Hughes and Proctor, 1988): the core (occupying 25% by radius), the radiative zone (accounting for 45 % of the Sun's radius), and the convective zone filling up the final 30% of the Sun's radius), where the radius of the Sun (R) is 6.96 × 105 km (Hotta and Yokoyama, 2011).

The core is a region in the Sun's center where there is a continuous Hydrogen-Hydrogen chain reaction through a thermo-nuclear reaction process converting hydrogen into helium (Gombosi and Holman, 1999). Energy produced through nuclear fusion in the Sun's core drives Solar activities and is the source of all of the heat and light received on Earth (Hughes and Proctor, 1988). The temperature and density decrease outside the center of the Sun. The radiative zone surrounds the core, and is a transparent zone that photons can pass through. The high-energy gamma-ray photons move around continuously while passing through this zone. Some are absorbed, re-emitted, and returned to the core (Haigh, 2007), and in this journey, the photons may take around 10 million years to get through the radiative zone. The temperature and density are about 1.5 million degrees and 0.2g cm−3 respectfully at the outermost boundary of the radiative zone.

This boundary is called the interface layer or tachocline (Forgács-Dajka, 2004; Parfrey and Menou, 2007). It is theorized that the Sun's magnetic field is generated by the magnetic dynamo in this layer (Charbonneau, 2010). The fluid flow velocities change across the layer can stretch magnetic field lines of force and make them stronger.

The convective zone is the third and final region of the solar interior. In this region, energy is carried to the surface by a process of convection. It extends from a depth of about 10,000 km up to the visible surface and occupies about 30% of the Sun's radius (Durney and Spruit, 1980). In this zone, plasma gas, heated by the radiative zone beneath, rises in giant convection currents to the surface. Once the plasma gets to the surface of the Sun, it loses energy, cools and is recycled back to the base of the convection zone, where it gets more heat from the top of the radiative zone. The process then repeats itself (Nandy, 2006).

These various layers are illustrated in figure 2.3 below;

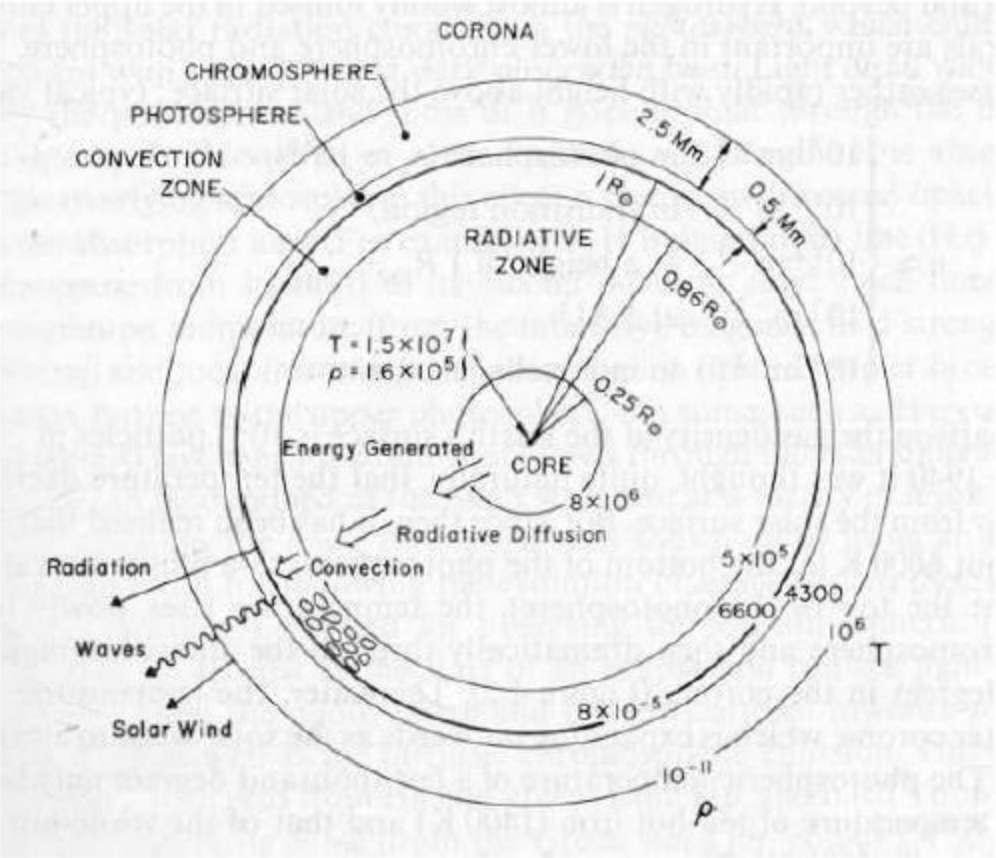

Figure 2.2*: The overall structure of the sun showing the sizes of different regions and their temperatures and densities (Rudraiah and Venkatachalappa, 1972)*

The photons escaping from the Sun, have lost energy on their way up from the core and changed their wavelength so most emission is in the visible region of the electromagnetic spectrum. The convective zone operates in lower temperatures thereby allowing heavier ions such as carbon to keep some of their electrons. This causes the material to be more opaque making it harder for radiation to get through, rather it totally absorbed. This causes heat to be trapped and ultimately makes the fluid unstable and it starts to boil or convect (Haigh, 2007).

2.2.2 Solar Atmosphere

The solar atmosphere is the observable part of the Sun which surrounds the unobservable interior. It contains regions that vary in temperature and density such as the photosphere, chromosphere, transition region, and corona. From the name it implies, the photosphere is the

sphere of light which is a thin shell of hot ionized plasma about 400 km thick, the bottom of which forms the visible surface of the Sun (Wilkinson, 2012). Below this layer, plasma is so opaque that it is impossible to see through (Janssen and Cauzzi, 2006)

The photosphere serves as a boundary between the Sun's interior (opaque region) and overlaying relatively transparent material called the solar atmosphere. Various features such as sunspots, bright features such as granules are observed on the photosphere. It is the source of most of the solar radiation. The visible (VIS:400-800 nm), UV, and infrared (IR) radiation comes from the photosphere. In the photosphere, the temperature (T), as well as the density, decreases with increasing height. The temperature of the photosphere varies between about 6500 K at the bottom and 4000 K at the top (Ossendrijver, 2003) and its minimum temperature serves to mark the base of the next layer: the chromosphere. Unlike the layers below the solar surface, in the atmosphere, radiation rather than convection is the dominant mode of energy transportation (Babatunde, 2006; Howard, 1978) (Wiegelmann et al., 2014).

The layer of the Sun's atmosphere immediately above the photosphere is the chromosphere. This layer has a density much less than that of the photosphere. The chromosphere is more transparent than the photosphere. The temperature in the chromosphere varies between about 4000 K at the bottom and 8000 K at the top. Density decreases continuously by height in the chromosphere, but temperature which reaches a minimum at the top of the photosphere increases slowly and reaches a value of 9,000 K at 2,000km (Koskinen, 1998; Rodger, 1998). The chromosphere is the site of solar flares, these flares sometimes appear as a sudden brightening of an existing plage (a bright patchy region within the chromosphere). They are also known to eject particles of matter in addition to electromagnetic radiation. Flares are associated with sunspot groups. During a solar flare, temperatures in a compact region reach five million degrees. Such flares usually last for 20 minutes. Ultraviolet and x-ray radiation from a flare takes about 8 minutes to reach Earth, while high energy particles from them arrive a day or two later (Du, 2015; Korsós, 2018).

The transition zone is relatively shallow but the temperature increases several orders of magnitude to around a million degrees. Above the transition zone is the corona, the outer atmosphere of the Sun. It can only be seen during a total solar eclipse. It appears as white streamers or plumes of ionized gas that flow outward into space (Glencross, 1981).

2.3 Solar Irradiance

The total amount of radiation received from the Sun at normal incidence at the top of the earth's atmosphere, at the mean sun-earth distance, is referred to as the Total Solar Irradiance (TSI) or extraterrestrial solar irradiance. The TSI varies over time, albeit by a small amount, and its magnitude and variations directly or indirectly affect many atmospheric and biological processes on earth. Following the work of (Gueymard, 2004) an estimate of the mean TSI for the above period is made. Applying a 27-day smoothing filter (with missing data substituted with the mean of the data for the last day before and the first day after the observed gap), the maximum and minimum values become 1367.1 Wm−2 and 1364.8 Wm−2, respectively, yielding a mean value of 1365.9 ± 1.4 Wm−2 (Darula et al., 2005) The total output power of the sun is about 3.846×1026 W, known as solar luminosity (Ball, 2012). It is the radiative power emitted over the entire surface of the Sun. Irradiance is the quantity that a solar radiometer observes at the annual mean Sun-Earth distance (Iorio, 2011) of one astronomical unit (1AU = 1.496 × 1011m).

The absolute level of TSI was previously accepted by the solar science community to be approximately 1365 Wm 2 0.15% (Crommelynck et al., 1995). However, the SOlar Radiation and Climate Experiment (SORCE) satellite with onboard Total Irradiance Monitor (TIM) launched in 2003 had provided a new absolute TSI value which was approximately 5 Wm−2 lower than the previous value (Kopp and Lean, 2011). In their calibration, they showed that the TSI value of 1360.8 ± 0.5Wm−2 is the best representative value of solar minimum. The spectral distribution of stars can be approximated as a black body.

Solar Irradiance is the incoming radiant flux per unit area incident on the surface Earth in the form of electromagnetic radiation produced by the Sun (Apell and McNeill, 2019; Lawin et al., 2019). Given that incoming Solar radiation is a vital energy supply to Earth, it is important we understand and model the amount of solar irradiance we receive. In other words, solar irradiance is the output of light energy from the entire disk of the Sun, measured at the Earth's atmosphere (Apell and McNeill, 2019; Cachorro et al., 1997; Michalsky et al., 1999).

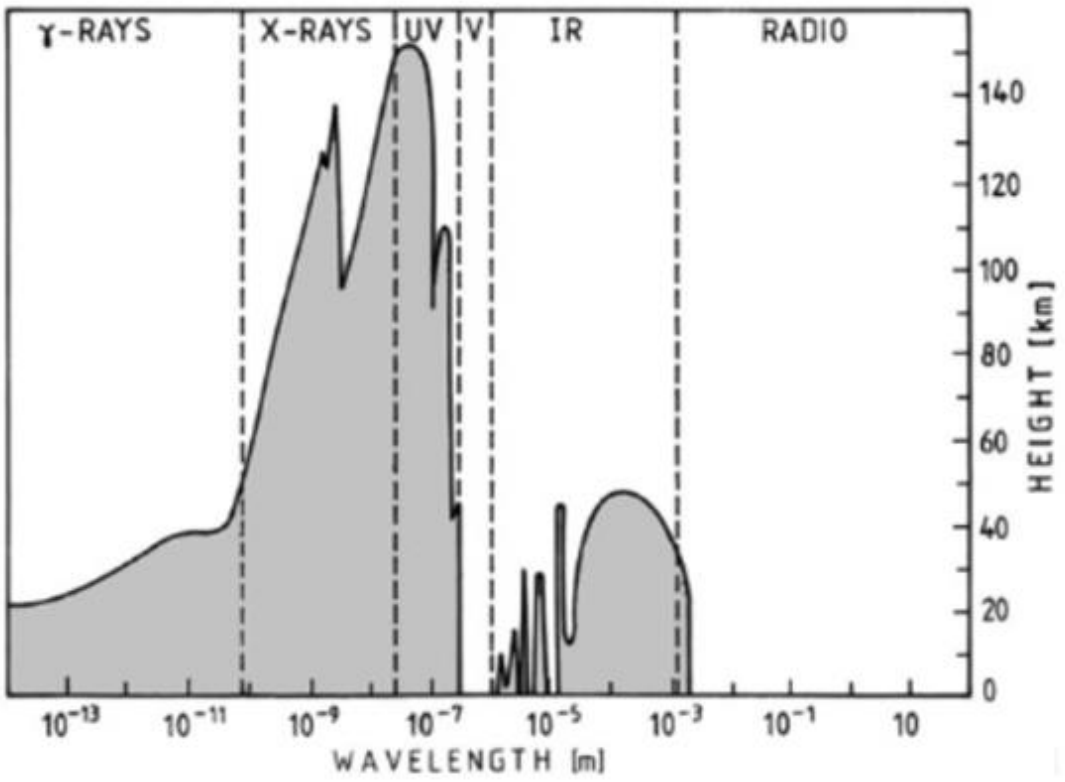

Figure 2.3*: Absorption of solar radiation by the Earth's atmosphere. The shaded areas provide the height above ground where the incoming intensity is reduced to 50% of its original strength. [Nicolson (1982), Stix (2004)]*

The atmosphere of Earth is very important in the total amount of solar irradiance reaching the Earth's surface, because it causes the attenuation of incoming solar radiation through scattering and absorption processes as shown in Figure 2.3 above. These phenomena are known as radiative transfer (Gueymard, 2012; Gueymard and Ruiz-Arias, 2015). (Michalsky et al., 1999) asserts that as the atmosphere is a very dynamic system varying with geographical location and altitude, a model is needed to provide a reasonable estimate of the solar irradiance spectrum. The most important variables in solar energy are solar irradiance and surface air temperature compared with other climatic and environmental factors (Gueymard, 2012; Lawin et al., 2019).

However, solar spectral irradiance is a measure of the brightness of the entire Sun at a wavelength of light. The solar irradiance spectrum is the spectral distribution of incident solar flux reaching the surface of the Earth. This spectrum spans the ultraviolet region, visible region to the near-infrared, and peaks about the visible region (Gueymard and Ruiz-Arias, 2015). A applications,

such as agriculture, remote sensing, oceanic studies, climatic studies, and solar energy harvesting industries require a reasonable prediction of solar spectral irradiance as the ability and practicability of actual measurements may not always be a possibility. (Blanc et al., 2014; Lawin et al., 2019; Wielicki et al., 1998) have carried out many studies that highlight the changes, trends, and variability analysis of the solar spectral irradiance and temperature. This knowledge is important for climatic studies as ocean waters have a huge impact on extreme weather in coastal areas and the thermal expansion of seawater. Due to the inaccessibility of certain remote areas for actual measurements (Gueymard, 2012), then a need for the development of solar spectral irradiance models was deemed a necessity.

2.3.1 Blackbody Radiation Body

The radiation from the Sun went out in the form of Electromagnetic radiation in the energy of an integral multiple of E = hν. The photons that making up the electromagnetic field have energies E = hν. Thus, Planck arrived at the Planck energy distribution for the radiation as a function of Energy E, IEdE emitted by the black body with energies between E and

$$E + dE \tag{2.1}$$

T is the absolute temperature of the black body and k is the Boltzmann constant. In Equation (2.1), the flux is given as a function of the energy E. We are interested in flux as a function of wavelength λ.

$$I_\lambda d\lambda = \frac{2\pi hc^2}{\lambda^5} \frac{1}{e^{hc/\lambda kT} - 1} d\lambda \tag{2.2}$$

where $I_\lambda d\lambda$ again is the radiation energy with wavelengths between λ and $\lambda + d\lambda$. passing a square meter per second [Wm^{-2}]. For large frequencies or small wavelengths λ the (1) in the denominator may be ignored and one finds the peak value of the flux I_λ as

$$\lambda_{max} T = 2898 \tag{2.3}$$

This approximate, but useful relation is called Wiens displacement law. By integrating Equation (2.2) overall energies, one finds another well-known equation, Stefan-Boltzmann

law. This law shows how the total flux I [Wm−2] emitted by a black body depends on its temperature.

$$I(T) = \sigma T^4 \tag{2.4}$$

Here, σ is the Stefan-Boltzmann constant, independent of the material. Given the shape of the curves, it appears to emit a smooth spectrum with the intensity I as a function of wavelength λ shown in Figure 2.4. The position of the peak shifts to higher wavelengths for lower temperatures.

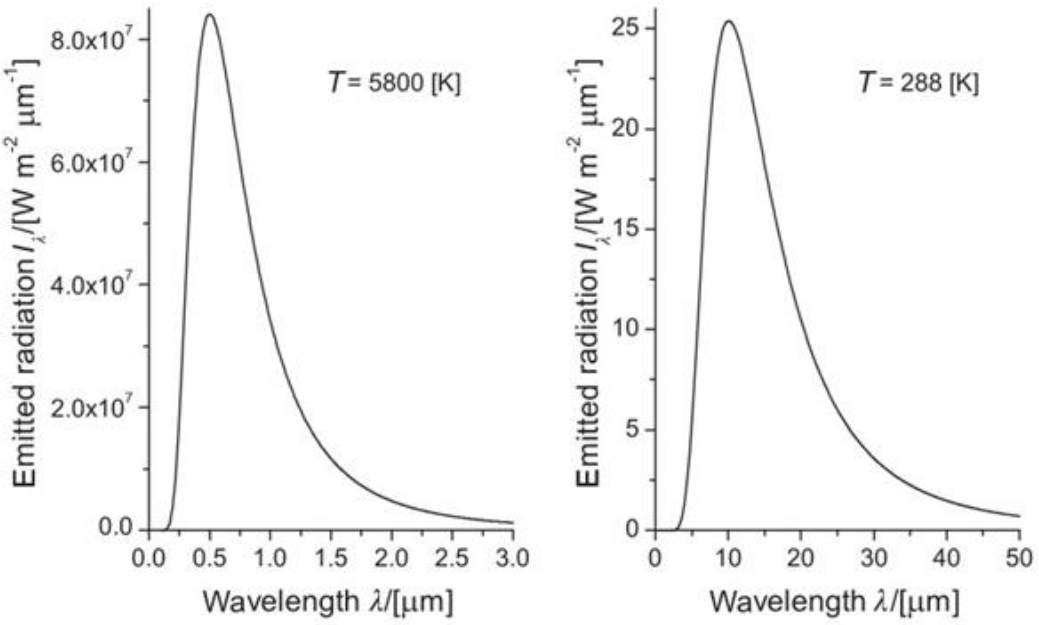

Figure 2.4*: Blackbody radiation* (Janssen and Cauzzi, 2006)

2.3.2 Emission Spectrum of the Sun

The electromagnetic spectrum given off by the sun encompasses all types of radiation as shown in table 2.1 below;

Class			Wave-length λ	Freq-uency f	Energy per photon E
Ionizing radiation	γ	Gamma rays	1 pm	300 EHz	1.24 MeV
	HX	Hard X-rays	10 pm	30 EHz	124 keV
	SX	Soft X-rays	100 pm	3 EHz	12.4 keV
			1 nm	300 PHz	1.24 keV
	EUV	Extreme ultraviolet	10 nm	30 PHz	124 eV
	NUV	Near ultraviolet, visible	100 nm	3 PHz	12.4 eV
			1 μm	300 THz	1.24 eV
	NIR	Near infrared	10 μm	30 THz	124 meV
	MIR	Mid infrared	100 μm	3 THz	12.4 meV
	FIR	Far infrared	1 mm	300 GHz	1.24 meV
Micro-waves and radio waves	EHF	Extremely high frequency	1 cm	30 GHz	124 μeV
	SHF	Super high frequency	1 dm	3 GHz	12.4 μeV
	UHF	Ultra high frequency	1 m	300 MHz	1.24 μeV
	VHF	Very high frequency	10 m	30 MHz	124 neV
	HF	High frequency	100 m	3 MHz	12.4 neV
	MF	Medium frequency	1 km	300 kHz	1.24 neV
	LF	Low frequency	10 km	30 kHz	124 peV
	VLF	Very low frequency	100 km	3 kHz	12.4 peV
	ULF	Ultra low frequency	1000 km	300 Hz	1.24 peV
	SLF	Super low frequency	10000 km	30 Hz	124 feV
	ELF	Extremely low frequency	100000 km	3 Hz	12.4 feV

Table 2.1: *The electromagnetic spectrum* (Aschwanden, 2011)

The part of the spectrum reaching the surface of Earth from the sun falls in the range of 100 nm and 1 mm. This range is broken into three: visible, infrared and ultraviolet radiation . Visible light falls has a range of 400-700 nm, and infrared light from about 700 nm to just

over 1 mm. Colors are determined by the length in the visible light spectrum, longer wavelengths look red while shorter wavelengths are blue as they range closer to the ultraviolet spectrum (Aschwanden, 2011).Ultraviolet contains wavelengths between 100-400 nm. . . Ultraviolet radiation can be divided into three distinct wavelength ranges: UV-A, UV-B and UV-C. These can directly affect the DNA of water inhabitants, because as the wavelength range gets shorter, it is capable of causing more damage.

Wavelengths between 100 and 280 nm fall in the UV-C range. This range makes up about 0.5% of all solar radiation, but can cause the most damage. However, most of this radiation is absorbed by stratospheric ozone, and very little gets to the surface. UV-B (280-320 nm) is an energetic, photo-activating radiation that is partially absorbed in the stratosphere. It is known for causing skin cancer in humans, and can impair photosynthesis in many plants (Sandorfy, 1979). The depth that UV-B penetrates water depends on water chemistry and turbidity . It can reach greater depths in saline water as deep as 20m below the surface of the ocean than in freshwater (Gilgen, 1998). UV-A (320-400 nm) also called blacklight has less energy than UV-B, and is not absorbed by ozone in the atmosphere. However, cloud cover can block it from reaching the surface. It is known for its ability to cause fluorescence in some materials (Sage, 2012). While UV-A is absorbed less readily by water, it can penetrate deeper than UV-B and UV-C. It is responsible for sunburns in humans (Michalsky et al., 1999).

Visible light cuts across the electromagnetic spectrum from blue to red, blue light has a higher energy and shorter wavelength than red. The lowest energy in the visible spectrum belongs to red light (Kohn, 1989). As visible light reaches Earth, surfaces produce visible colors by absorbing or reflecting different wavelengths. The color that a surface appears to be depends on the wavelength reflected by the surface, and it will appear white if all of the visible wavelengths are reflected (Gilgen, 1998).

Infrared radiation has a wavelength greater than 700 nm and provides 49.4% of solar energy. It is readily absorbed by water and carbon dioxide molecules and converted to heat energy (Kellner, 1942). Longer wavelengths excite electrons in the substances that absorb them causing heat and it is responsible for warming Earth's surface. Infrared light due to its

longer wavelengths is reflected more than UV or visible light. This reflection allows infrared radiation to transfer heat between the surface, water and the air (Kawamoto and Hayasaka, 2008).

2.3.3 Solar Energy interface

Solar irradiation is not exhaustible on the time scale humans. The sustainability of sources of renewable energy, one has to perform a life-cycle process. Fig. 2.5 shows the temperature of the earth is determined by the incoming solar radiation and the infrared radiation leaving the earth or

$$Energy\ in\ =\ Energy\ out \tag{2.5}$$

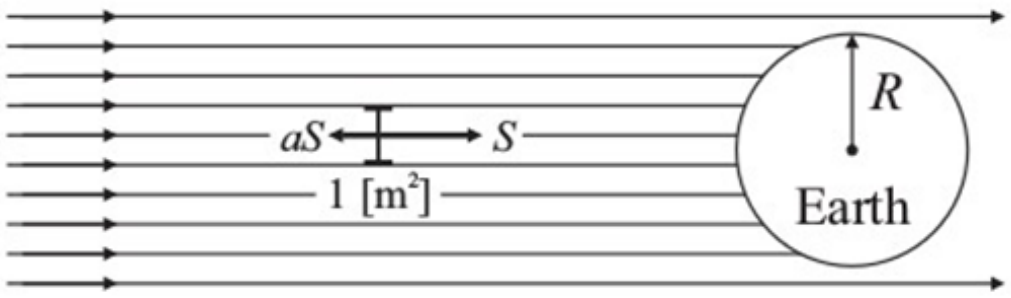

Figure 2.5*: Solar radiation is entering the atmosphere from the left, S [W/m2]. A fraction called the albedo a, is reflected back*

2.3.4 Solar Energy

The total amount of radiation entering the Earth's atmosphere per meter square perpendicular to the radiation is called I, the total solar irradiance or solar constant in units of Watts per meter square.

Solar irradiance, an amount of;

$$I = (1 - a)I_o \tag{2.6}$$

penetrates down to the earth's atmosphere, with Earth radius R an amount of;

$$Energy\ in = (1 - a)I_o \pi R^2 \quad (2.7)$$

We take the Earth as a black body with temperature T, to estimate the right-hand side of Eq. 2.7. A black body can be defined as a hypothetical body, which absorbs all incoming radiation, acquires a certain temperature T. The total radiation leaving the earth then becomes;

$$Energy\ out = \sigma T^4 4\pi R^2 \quad (2.8)$$

Then Equation (2.1), becomes;

$$(1 - a)I_o = 4\sigma T^4 \quad (2.9)$$

2.3.5 Atmospheric Effect on Solar radiation

The Earth's atmosphere has several impacts on the solar radiation reaching the surface. They include:

1. A decrease in solar radiation power due to absorption, scattering, and reflection in the atmosphere
2. Atmospheric variations such as clouds, pollution, and aerosols have a further effect on the power, spectrum, and incident direction
3. Spectral content change of the solar radiation as a result of higher absorption or scattering of some wavelengths more than others, and;
4. The introduction of an indirect component into the solar radiation;

As solar radiation passes through the atmosphere, its constituents absorb the incident photons. A very high absorption of photons that have energies close to the bond energies of atmospheric gases such as ozone (O3), carbon dioxide (CO2), and water vapor (H2O). This absorption leads to deep troughs in the spectral radiation curve. Carbon dioxide and water vapor absorb majority of the far-infrared above 2 μm . Similarly, ozone absorbs most of the ultraviolet light below 0.3 μm (Kellner, 1942; Sandorfy, 1976).

While atmospheric absorption by specific gases alters the spectral content of inbound solar radiation, they have little impact on the overall power. Rather, reduction in the power occurs when air molecules and dust absorb and scatter light. Deep troughs in the spectral irradiance curve are not caused by this absorption process, but instead a reduction in power dependent on the path length through the atmosphere. (Chruścińska, 2013; Ovechkin et al., 1970). When the sun is overhead, the incident light appears white because absorption due to atmospheric constituents leads to a relatively uniform reduction across the visible spectrum. Higher energy (lower wavelength) light is absorbed and scattered more for longer path lengths. As a result, the sun appears much redder in the morning and evening, and has a lower intensity than in the midday (Crisp, 1997; Míguez, 2015).

The emission spectrum of the sun is shown in figure 2.6 as it enters the top of the atmosphere; the lower and more structured curve represents the solar spectrum as it is observed at sea level. The difference is due to the absorption of solar light in the earth's atmosphere. The gases mainly responsible for this absorption are indicated: CO_2, water vapor H_2O, O_2 and O_3.

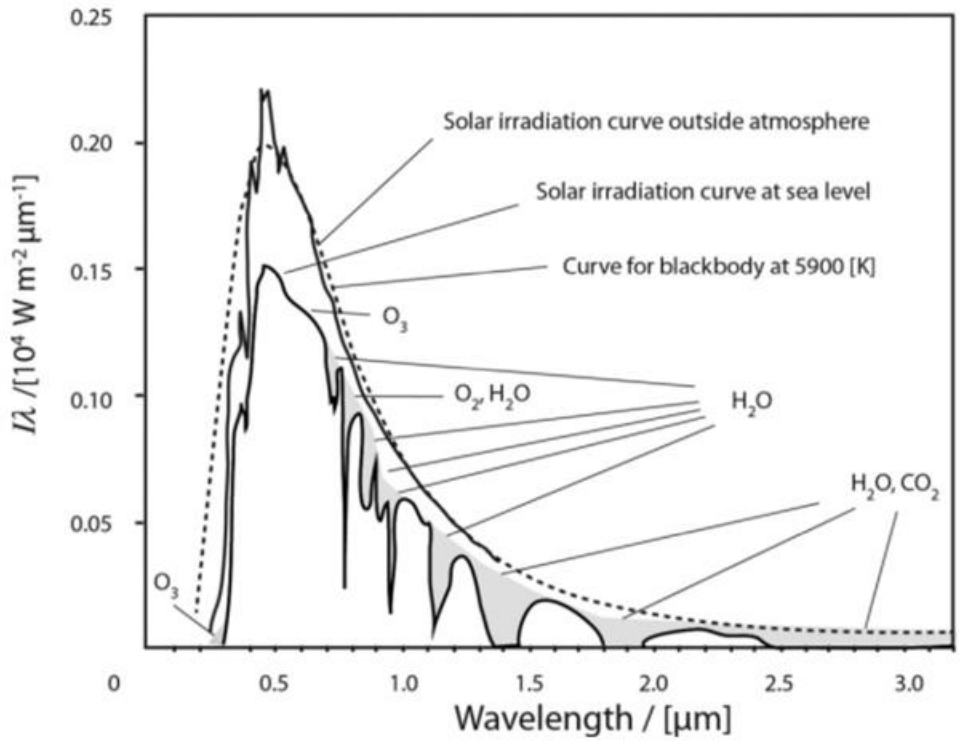

Figure 2.6: *Solar radiation incident on earth's atmosphere* (Míguez, 2015)

2.4 Components of Solar Irradiance

The inbound solar radiation consists of the following components;

1. Global Horizontal Irradiance
2. Diffuse Horizontal Irradiance
3. Direct Normal Irradiance

2.4.1 Global Horizontal Irradiance

Global Horizontal Irradiance (GHI) is defined as the total amount of shortwave radiation received from above by a surface horizontal to the ground (Gilgen et al., 1998; Pace et al., 2006; Reno and Hansen, 2016). This irradiance has great application in photovoltaic installations and is the sum of Direct Normal Irradiance (DNI) and Diffuse Horizontal Irradiance (DIF) and ground-reflected radiation (Lawin et al., 2019; Reno and Hansen, 2016).

$$GHI = DfHI + DNI * cos(z) \tag{2.10}$$

where *DfHI* is the diffuse horizontal irradiance, *DNI* is the direct normal irradiance, and *z* is the solar zenith angle

2.4.2 Diffuse Horizontal Irradiance

Diffuse Horizontal Irradiance (DHI), is the radiation at the Earth's surface from light scattered by the atmosphere. This Solar radiation arrives on a indirect path from the sun, after been scattered by molecules in the atmosphere and comes from all directions (Pace et al., 2006; Reno and Hansen, 2016). Figure 2.7 below illustrates the diffuse horizontal irradiance;

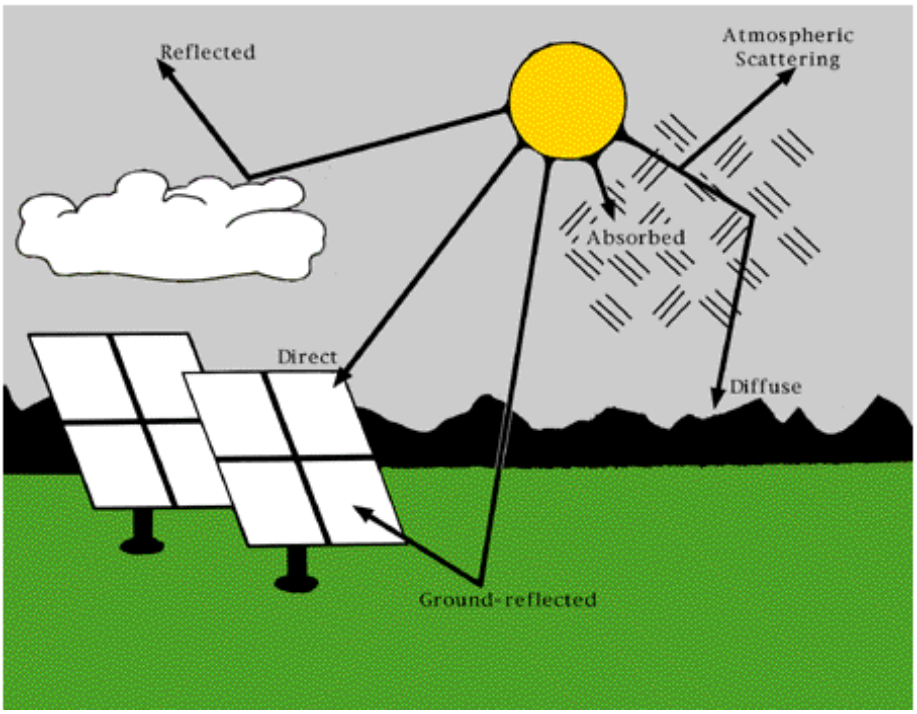

Figure 2.7*: Effects of the atmosphere on irradiance*

2.4.3 Direct Normal Irradiance

Direct Normal Irradiation (DNI) is also known as Direct Beam Irradiance, which is the total amount of radiation incident per unit area by a collecting surface held perpendicular to the incident radiation in a straight line from the Sun's position in the sky (Gueymard and Ruiz-Arias, 2015; Tolento and Robinson, 2019). Generally, the amount of irradiance annually received by a surface can be maximized by keeping it perpendicular to incident radiation. This quantity is of importance solar thermal installations and installations that track the position of the sun (Wielicki et al., 1998).

According to (Blanc et al., 2014), DNI is an essential component of global irradiance, especially under cloudless conditions, and represents the solar resource that can be used by various forms of Concentrating Solar Technologies (CST), such as concentrating solar power (CSP) systems - also called solar thermal electricity systems, including parabolic dish, parabolic trough.

The shortwave direct beam irradiance is calculated using spectral transmittance functions for main extinction processes in a cloudless atmosphere (Blanc et al., 2014; Wielicki et al., 1996;

Wielicki et al., 1998). These extinction processes include Rayleigh scattering, ozone extinction, nitrogen dioxide extinction, mixed gases extinction, water vapor extinction, and aerosol extinction and are represented by their respective transmittance functions T in the equation 2.11 below (Gueymard and Ruiz-Arias, 2015; Tolento and Robinson, 2019)

$$E_{bn\lambda} = E_{on\lambda} T_{R\lambda} T_{o\lambda} T_{n\lambda} T_{g\lambda} T_{w\lambda} T_{a\lambda} \quad (2.11)$$

Where $E_{bn\lambda}$ is the solar shortwave direct beam irradiance, $E_{on\lambda}$ is the extraterrestrial irradiance corrected for actual Earth-Sun system, $T_{R\lambda}$ is the Rayleigh scattering, $T_{o\lambda}$ is the ozone absorption, $T_{n\lambda}$ is the mixed gases absorption, $T_{g\lambda}$ is the trace gases absorption, $T_{w\lambda}$ is the water vapor absorption, and $T_{a\lambda}$ is the aerosol extinction. The general forms of the various transmittance functions T are modeled by the Beer-Lambert-Bouguer law.

2.5 Modeling of Solar Irradiance

To date, there have been many solar spectral irradiance models developed, each adopting a different approach to understand and compute the amount of solar radiation transmitted through the atmosphere. According to Gueymard (2005) and Seidel et al. (2010), the basic analytical models are based on the theory of radiative transfer and solved using simplified assumptions. More practical models are similarly based on the theory of radiative transfer. However, they depend on numerical methods (Lawin et al., 2019) and rigorous codes to solve the equation of radiative transfer at different layers of the atmosphere (Michalsky et al., 1999). The radiative transfer code is built on the parameterization of spectral transmittance functions of main extinction processes in the atmosphere. SMARTS or the Simple Model of Atmospheric Radiative Transfer (Gueymard and Ruiz-Arias, 2015) is an example of such a model.

The modeling of solar spectral radiation is an essential component of a large number of applications in many scientific disciplines. Gilgen et al. (1998) surmises that in solar applications, the spectral domains of interest cover the UV-A and UV-B band, visible band, and near-infrared band. These three bands combined constitute what is usually referred to as the shortwave spectrum. As such the accurate predictions of incident solar radiation are necessary for many different disciplines (Pinker et al., 1995), not just solar energy applications. A variety of applications spread

across different disciplines need spectral solar irradiance models (Kaskaoutis and Kambezidis, 2008a, 2008b; Tolento and Robinson, 2019) such as atmospheric science, biology, health physics, and energy technology (photovoltaic systems, high-performance glazings, daylighting, selective coatings, etc.). (Anmeng et al., 2019) showed that there are 12 possible uses of the solar spectral radiation models in building and solar energy system applications.

In recent years, Apell and McNeill (2019) asserts that many solar spectral irradiance models have been developed, and these spectral models provide considerably more flexibility, and normally better accuracy because of the more physical nature of their modeling. These models vary from numerical codes (Gueymard, 2005), parameterized functions to empirical models. Numerical code such as MODTRAN simulates the atmosphere with atmospheric parameters (Gueymard, 2004, 2005) such as temperature, pressure, and extinction coefficients defined for each layer and uses numerical methods to calculate diffuse irradiance, while the scientific and engineering models such as Simple Model of Atmospheric Radiative Transfer of Sunshine (SMARTS) and SPECTRAL rely on the parameterization of various transmittance functions, working based on MODTRAN codes with a more user-friendly interface (Gueymard, 2005). So, in other words, there are two types of solar spectral irradiance models that may be used to analyze or predict solar radiation at the Earth's surface (Badescu, 1997; Ineichen, 2016; Tolento and Robinson, 2019). They are as follows;

1. The sophisticated rigorous codes, which takes into account the vertical atmospheric inhomogeneity through a series of superimposed scattering and absorbing layers, and;
2. Simple atmospheric transmittance parameterizations in which the atmosphere is approximated as a one-layer medium attenuating the extraterrestrial solar irradiance by means of several scattering and absorption processes.

The main model used in this research study is the SMARTS model, which was originally developed to investigate the effect of varying atmospheric conditions on the performance of spectrally selective glazing, but the model evolved into a versatile radiative transfer code adaptable to a variety of applications. It is agreeable that in recent years, this model has received considerable improvements and will be subjected to extensive discussion in the next subsection.

2.5.1 SMARTS Spectral Model

SMARTS, an acronym for Simple Model of the Atmospheric Radiative Transfer of Sunshine, is a complex but versatile model that requires significant experience and knowledge of basic physics and meteorology. SMARTS is basically a program designed to evaluate the surface solar irradiance components in the spectral range 280 to 4000 nm (shortwave spectrum) under cloudless conditions (Xiao et al., 2014). Gueymard (2005) asserts that the program, based on FORTRAN, relies on simplifications of the equation of radiative transfer to allow fast calculations of surface irradiance.

Solar energy researchers use SMARTS to test the performance of spectroradiometers, develop reference spectra, establish uniform testing conditions for materials research, optimize daylighting techniques, and verify broadband radiation models (Gueymard, 2019). SMARTS is used in the fields of architecture, atmospheric science, photobiology, and health physics. SMARTS is used for example to evaluate the energy production of solar panels under variable atmospheric conditions (Gueymard, 2004; Kaskaoutis and Kambezidis, 2008a, 2008b).

Because Earth's atmosphere is a continuously changing filter that modifies the sunlight that travels through it. SMARTS can be used to predict the cloudless direct, diffuse, global, and circumsolar irradiance on any horizontal or tilted surface at wavelengths from 280 to 4000 nm. Otherwise stated, SMARTS predicts clear-sky spectral irradiances and computes how atmospheric changes affect the photon energy for each wavelength of light.

The primary logical use of a spectral model is to predict terrestrial spectra for applications that involve highly spectrally selective natural phenomena or artificial processes (Xiao et al., 2014). The primary purpose of the SMARTS code is to be as versatile as possible and therefore to address a variety of both spectral and broadband applications, through the use of its different options (Kaskaoutis and Kambezidis, 2008a, 2008b), and therefore has been used to discuss some current developments in various disciplines.

A characteristic of the SMART model is its versatility (Gueymard, 2005; Xiao et al., 2014), a huge number of applications in various disciplines are possible. This is achieved by having a number of options in addition to the core calculations. Other features of the model are (Kaskaoutis and Kambezidis, 2008a, 2008b; Xiao et al., 2014):

i. The spectral transmittance functions it uses accurate and regularly updated;

ii. It provides improved spectral resolution over existing transmittance models;

iii. It produces spectral irradiances comparable to MODTRAN predictions with far simpler inputs; and

iv. Its predictions can be directly compared to spectro-radiometric measurements using built-in functions.

2.5.2 CAMS McClear

The Copernicus Atmosphere Monitoring Service (CAMS) McClear Clear-Sky Irradiation service delivers time series of solar radiation that would be observed/received in a specific site in the world (horizontal plane at ground level) under cloud-free conditions, with a time step ranging from 1 min to 1 month (Wagner et al., 2021; Wandji Nyamsi et al., 2021). The Global, Direct, and Diffuse Horizontal Irradiation, as well as the Beam Normal Irradiation, are provided (Apell and McNeill, 2019).

The Copernicus Atmosphere Monitoring Service (CAMS) McClear Clear-Sky Irradiation service assimilates observational data to provide sustained retrospective and real-time global monitoring of greenhouse gases and aerosols. Daily global forecasts of atmospheric composition, detailed air-quality forecasts, and assessments for Europe, and key information on the long-range transport of atmospheric pollutants are provided (Kaskaoutis and Kambezidis, 2008a, 2008b; Wandji Nyamsi et al., 2021). Comprehensive web-based graphical products and gridded or time-series data are created on which downstream services are based. Feedback is being given to providers of in-situ data on the quality of their data and on future observational requirements (Lawin et al., 2019; Xiao et al., 2014).

One of the CAMS services is the provision of radiation values at the ground level, which fulfill the needs in national policy developments and the requirements of partly commercial downstream services, e.g., for planning, monitoring, efficiency improvements, and the integration of solar energy systems into energy supply grids. This model will be used to evaluate the performance of SMARTS.

CHAPTER THREE

METHODOLOGY

3.0 Introduction

For the project carried out, there was no experimental work carried out. Instead, it was mainly restricted to comparative analysis of Global Horizontal Irradiance and Direct Normal Irradiance data modeled using the Simple Model of the Atmospheric Radiative Transfer of Sunshine (SMARTS) and a satellite-based dataset of the Copernicus Atmosphere Monitoring Service (CAMS) McClear Clear-Sky Irradiation service.

3.1 Description of Study Area

The focus of this study is limited to Ilorin, Kwara State, Central Nigeria. It is an urban metropolis and is the capital of Kwara State. The study site is situated at a latitude of 8.484°N, a longitude of 4.675°E, at an elevation of 400m above sea level. According to the Köppen classification, Ilorin is in the tropical savanna climate zone (Aw) with dry winter characteristics (Beck *et al*., 2020). Ilorin has an average precipitation rate of about 1217 mm and varies by 222 mm between peak and light rainy season months (Yusuf *et al*., 2021). Geographically, it is situated in central Nigeria at the Intertropical Convergence Zone (ITCZ) between the monsoon from the South Atlantic Ocean (Gulf of Guinea), and the tropical continental air mass from the northern Sahara deserts (N'Datchoh *et al*., 2017). The connection of two air masses, the impact of which varies during the year with the displacement of the intertropical convergence zone (ITCZ) (north-south) greatly affecting the climate in the study area. During the dry season months of November–February, hot and dry continental air masses leaving the Sahara Desert to give rise to the Harmattan twists over the majority of West Africa (N'Datchoh *et al*., 2017). The dust plumes can usually have a thickness of up to 3 km reducing the visibility to less than 1 km. This results in a reduction of surface solar radiation by a magnitude that is not well documented (Pinker *et al*., 2010). Moist air masses originating from the Atlantic Ocean bring annual monsoon rainfalls during the summer (Maloney and Shaman, 2008). The study site is labeled on the map of Nigeria in figure 3.1 below;

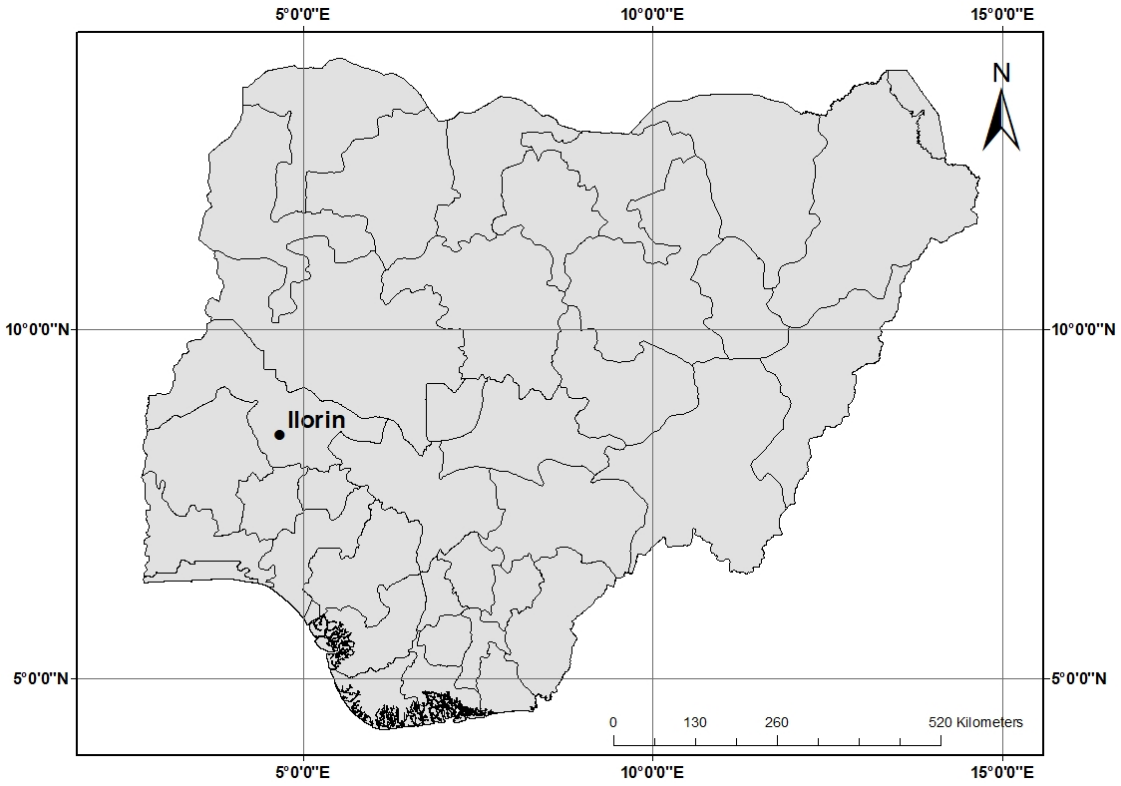

Figure 3.1: *Geographic location of the study site in Nigeria*

3.2 Sources of Data

The Direct Sun measurement and Aerosol inversion products data utilized in this study was obtained from the NASA AERONET (AErosol RObotic NETwork) station at the National Air Quality Laboratory, Department of Physics of the University of Ilorin, supported by the Center for Atmospheric Research, National Space Research & Development Agency (CAR-NASRDA), situated in Ilorin, Kwara State, Nigeria. This data can be accessed through the Goddard Space Flight Center AERONET portal https://aeronet.gsfc.nasa.gov/.

Satellite-based Irradiance data from the Copernicus Atmosphere Monitoring Service (CAMS) McClear Clear-Sky Irradiation service was also used in this study. The Clearness Index (KT) data was obtained from the National Aeronautics and Space Administration (NASA) Langley Research Center (LaRC) Prediction of Worldwide Energy Resource (POWER) Project funded through the NASA Earth Science/Applied Science Program.

3.2.1 Data Used

The study was carried out using the following data;

- Version 3 AERONET data computed for data quality level 1.5 (cloud-screened and quality controlled) under Almucantar Sky scan scenario
- The AERONET data includes: Precipitable Water, Angstrom Parameter, Aerosol Optical Depth at 500nm, Angstrom Exponent (380-500nm), Angstrom Exponent (500-870nm), Single Scattering Albedo (440nm), Asymmetry Factor (440nm) & Surface Albedo (440-1020nm)
- Global Horizontal Irradiance and the Direct Normal Irradiance (Beam) from the Copernicus Atmosphere Monitoring Service (CAMS) McClear Clear-Sky Irradiation service
- Copernicus Atmosphere Monitoring Service (CAMS) McClear Clear-Sky Irradiation service Global Horizontal Irradiance, Diffuse Horizontal Irradiance and the Direct Normal Irradiance (Beam)
- The Clearness Index (KT) data.

3.3 Data Collection instrument

The Cimel CE318 Sunphotometer is a multi-channel, automatic sun-and-sky scanning radiometer for the retrieval of essential physical-optical parameters at the Earth's surface. The physical dimensions are 128.5 cm x 150 cm x 101 cm and weigh approximately 10kg. This high-precision multiband photometer measures the optical properties of the atmosphere and provides the quantification and physical-optical characterizations of the aerosols. They measure the extent to which aerosols and water prevent the direct transmission of sunlight of a specific wavelength through the atmosphere. It makes two basic measurements, within several programmed sequences, either direct sun or sky. The direct sun measurements are made in eight spectral bands requiring approximately 10 seconds. Eight interference filters at wavelengths of 340, 380, 440, 500, 670, 870, 940 and 1020 nm are located in a filter wheel which is rotated by a direct drive stepping

motor. The 940 nm channel is used for column water abundance determination. Figure 3.2 below shows the data collection equipment;

Figure 3.2: *AERONET Cimel CE318 Sun photometer* (Pinker *et al*., 2010)

The photometer requires an unobstructed sight of the sun and the site should be clear of obstructions on the east-west transect at all angles. Measurements are taken at pre-determined discrete wavelengths in the visible and near-IR parts of the spectrum to determine atmospheric transmission and scattering properties. It takes measurements only during daylight hours (sun above the horizon). The robot mounted sensor head is parked pointed near-nadir when idle to prevent contamination of the optical windows from rain and foreign particles. This instrument is weather-proof and requires little maintenance during periods of adverse weather conditions.

3.4 Method of Data Generation and Analysis

The project was carried out using the publicly available Simple Model of the Atmospheric Radiative Transfer of Sunshine (SMARTS) model created by Dr. Christian Gueymard. It computes clear sky spectral irradiances for specified atmospheric conditions such as direct beam, circumsolar, diffuse, and total on a tilted or horizontal receiver plane.Users can specify conditions from any of the 10 standard atmospheres or their own data. SMARTS 2.9.5 is the basis for the American Society of Testing and Materials (ASTM) reference spectra (ASTM G-173 and ASTM G-177) for testing and materials degradation studies in photovoltaic performance. SMARTS can be used to predict the cloudless direct, diffuse, global, and circumsolar irradiance on any horizontal or tilted surface at 2002 wavelengths from 280 to 4000 nm. The SMARTS model was used to generate daily irradiance data one day at a time. A simplified flowchart of the SMARTS algorithm for modeling spectral irradiance is shown in Figure 3.3;

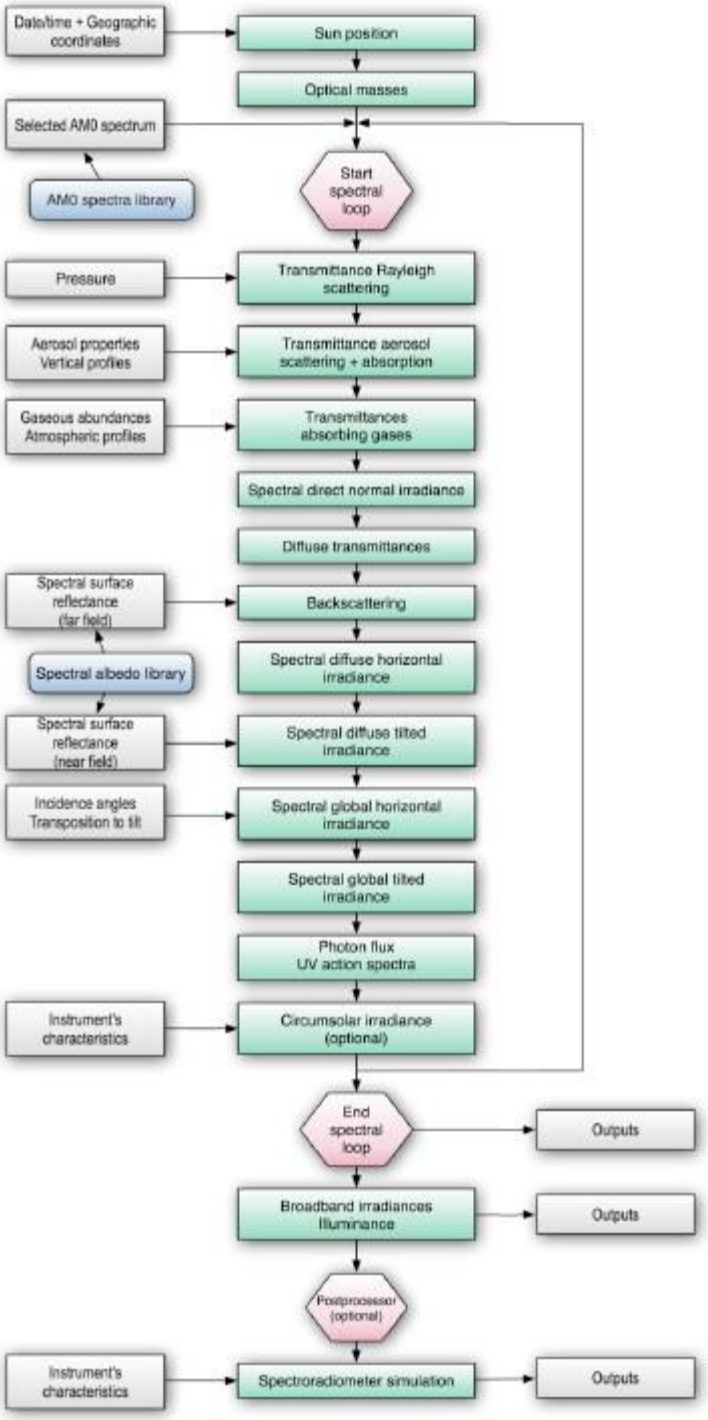

Figure 3.3: *Simplified flowchart of the SMARTS algorithm*

3.4.1 Configuration of SMARTS model

The SMARTS model was configured using the 19 configuration cards provided as shown in figure 3.4;

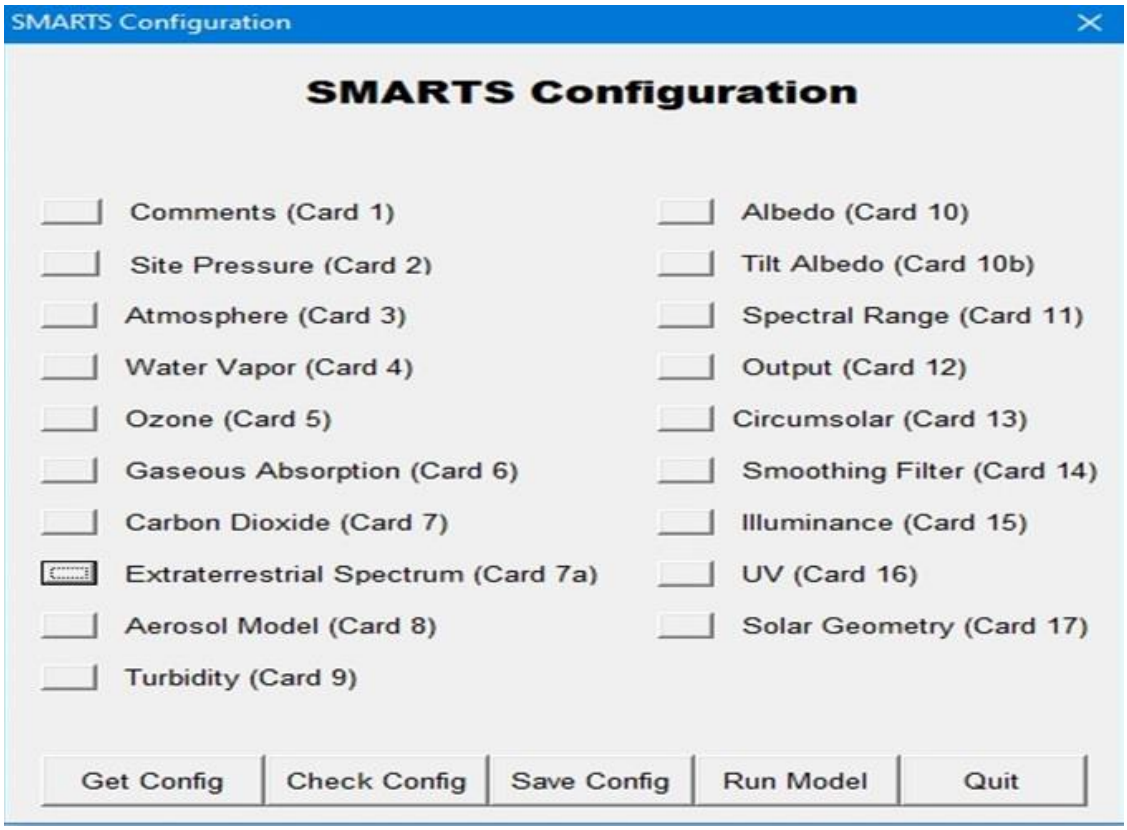

Figure 3.4: *SMARTS configuration*

1. **Comments (Card 1)**: This was used to label the irradiance data generated with the date.
2. **Site Pressure (Card 2)**: A site here refers to a simulated target at a fixed height above ground, with the ground at a fixed altitude above sea level. The total height and altitude must be less than 100 kilometers (km). Our study site Ilorin fits the requirement, and site pressure of 1013.25 millibars (mb) was used.
3. **Atmosphere (Card 3)**: A tropical reference atmosphere was selected to match the study site's atmospheric conditions.

4. **Water Vapor (Card 4)**: The Precipitable Water (cm) value of the day being simulated was specified from the AERONET data.

5. **Columnar Ozone Abundance (Card 5)**: The default from the reference atmosphere was used.

6. **Gaseous Absorption and Pollution (Card 6)**: The reference tropospheric condition was modified to "Pristine Atmosphere" to simulate a clear sky condition.

7. **Carbon Dioxide (Card 7)**: The Carbon Dioxide concentration in parts per million volume was set at 370 ppmv.

8. **Extraterrestrial Spectrum (Card 7a)**: The Gueymard (2004) reference was used here.

9. **Aerosol Model (Card 8)**: User model was used in this card with user-specified values of ALPHA1 (Angstrom wavelength exponent below 500nm), ALPHA2 (Angstrom wavelength exponent above 500nm), OMEGA (Single-scattering albedo), and G (Asymmetry factor). All values were retrieved from the AERONET data.

10. **Turbidity (Card 9)**: The value of the Aerosol Optical Depth at 500nm retrieved from AERONET data was inputted.

11. **Regional Albedo (Card 10)**: A fixed albedo was specified, with an average broadband value between 0 and 1.

12. **Tilted Surface & Local Albedo (Card 10b)**: The tilt calculations were bypassed for this card.

13. **Spectral Range & Solar Constant (Card 11)**: The Spectral range wavelength in nanometers (nm) was set at a minimum of 280 and a maximum of 4000. Solar Constant in Watts / metre^2 specified at 1366.1, with a Solar Constant Distance Correction Factor set at 1.0.

14. **Output (Card 12)**: This card was used to create .OUT and .EXT files, and to include the spectral results in the .EXT file only. The Spectral range was again stated, and an interval (step) of 0.5 was set.

15. **Circumsolar Calculations (Card 13)**: In this card, the bypass option was selected.
16. **Smoothing Filter (Card 14)**: Extra Scanning/Smoothing was bypassed in this card.
17. **Illuminance (Card 15)**: Extra Illuminance and Photosynthetically Active Radiation calculations were bypassed in this card.
18. **UV (Card 16)**: In this card, extra UV calculations were bypassed.
19. **Solar Geometry (Card 17)**: In this card, the inputted data were the year, month, day, hour, latitude, longitude, and time zone. The local standard time range was 06.00 - 18.00 hours in 24 hours format.

The configuration was then saved after which the model was run. A total of 13 hours of hourly data was gotten daily for 189 days of the year 2020. This gave a total of 2457 entry points in the dataset gotten from the SMARTS model for each type of irradiance.

3.5 Data Analysis Procedure

The results generated from the radiative transfer model were for each wavelength from 280 - 4000 nm, a sum of the values for this shortwave range was done before analysis began. The performance of the Simple Model of the Atmospheric Radiative Transfer of Sunshine (hereafter referred to as SMARTS) model estimates was evaluated against satellite-based observations from the Copernicus Atmosphere Monitoring Service (CAMS) McClear Clear-Sky Irradiation service (hereafter referred to as CAMS).

The hourly values of Global Horizontal Irradiance (GHI) and Direct Normal Irradiance (DNI) values for all the days of the year with available data between 1st January and 31 December 2020 obtained from the SMARTS were then paired with the respective GHI and DNI from the CAMS dataset. The time of the day was in hours ranging from 6.00 hours to 18.00 hours in local time (LT). The average hourly values of SMARTS irradiances were then plotted against those of CAMS in the earlier stated local time range to examine the hourly variation trends and how closely it was to CAMS.

This was done for the local wet and dry seasons. A monthly average comparison was also done while incorporating the Clearness index (KT) to discern how these irradiance were affected by it throughout the year. The plots of this study were done using a combination of MATLAB and Origin statistical software. The statistical data of the irradiance was compiled using the following equations;

$$Mean = \frac{1}{n}\sum_{i=1}^{n} x_i \tag{3.1}$$

$$\text{Standard Deviation} \quad (\sigma) = \sqrt{\frac{1}{n-1}\sum_{i=1}^{n}(x_i - \bar{x})^2} \tag{3.2}$$

$$\text{Standard Error of Mean} \quad = \frac{(\sigma)}{\sqrt{n}} \tag{3.3}$$

$$Bias = (\mathrm{X_{SMARTS}} - \mathrm{X_{CAMS}}) \tag{3.4}$$

$$\text{Relative Bias} \quad = \frac{(\mathrm{X_{SMARTS}} - \mathrm{X_{CAMS}})}{\mathrm{X_{CAMS}}} \tag{3.5}$$

$$RMS = \sqrt{\sum_{i=1}^{n} (X_{SMARTS} - X_{CAMS})^2} \tag{3.6}$$

$$RMSE = \sqrt{\frac{1}{n} \sum_{i=1}^{n} (X_{CAMS} - X_{SMARTS})^2} \tag{3.7}$$

In the next chapter we show and discuss the results.

CHAPTER FOUR

RESULTS & DISCUSSION

In this chapter, the results of this research work are shown. The seasonal variation of Direct Normal Irradiance (DNI) & Global Horizontal Irradiance (GHI) modeled from the Simple Model of the Atmospheric Radiative Transfer of Sunshine is compared with that of the Copernicus Atmosphere Monitoring Service (CAMS) McClear Clear-Sky Irradiation service over Ilorin, Nigeria. Afterward, the histograms and scatter plots were also plotted, and the monthly variation over the year 2020 was plotted with the Clearness index to investigate the relationship. The local seasons considered were the dry and wet (rainy) seasons.

4.1 Dry Season

The variation of shortwave solar irradiance during the dry season will be reviewed in this section. This season is characterized by having the least atmospheric vapor content and little to no rainfall. The dry season occurs in the months of January, February, March, November & December, in the study area. An average hourly value of irradiance was used for the plots shown from the next page;

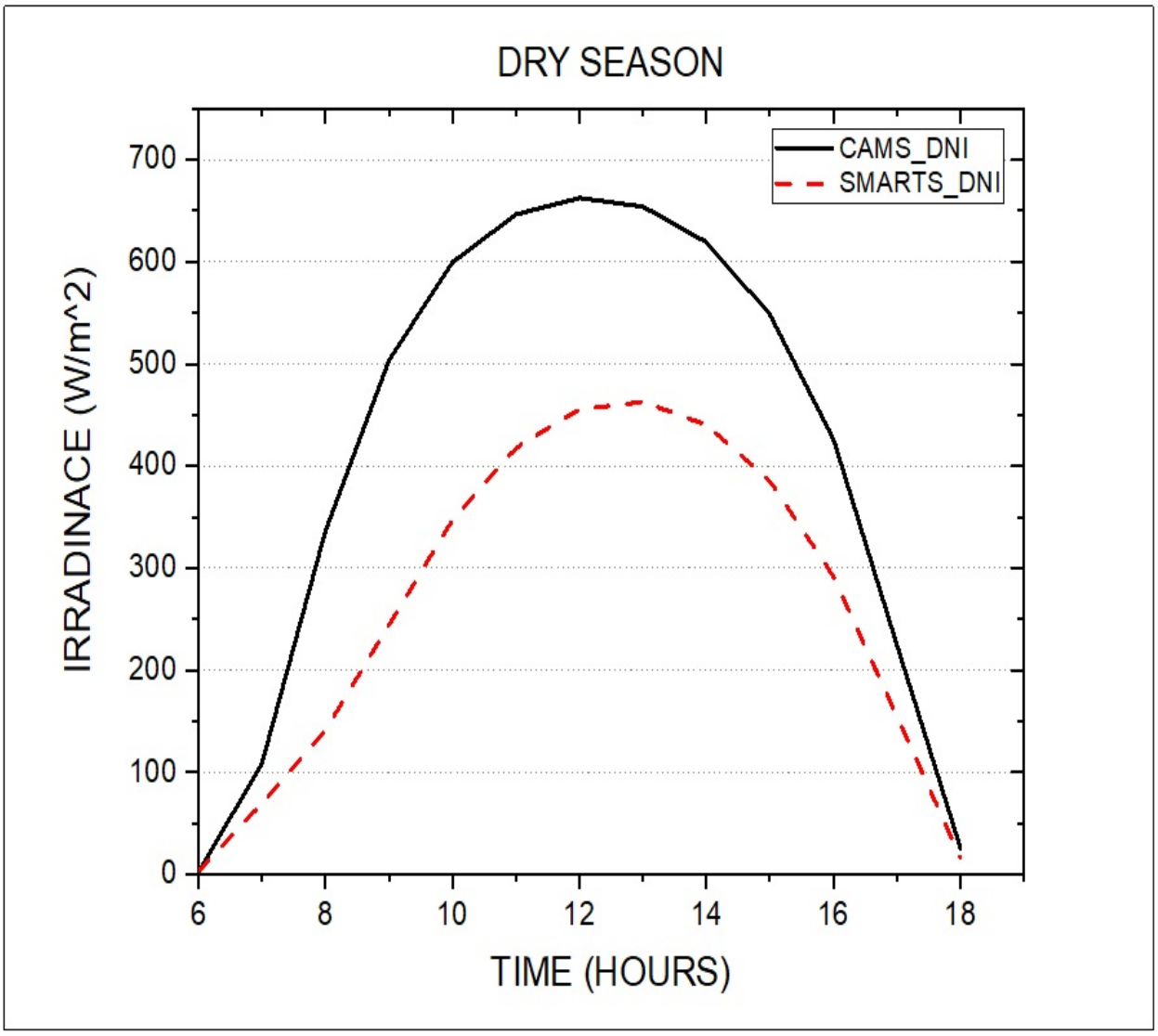

Figure 4.1: Hourly Average Direct Normal Irradiance plot in the dry season

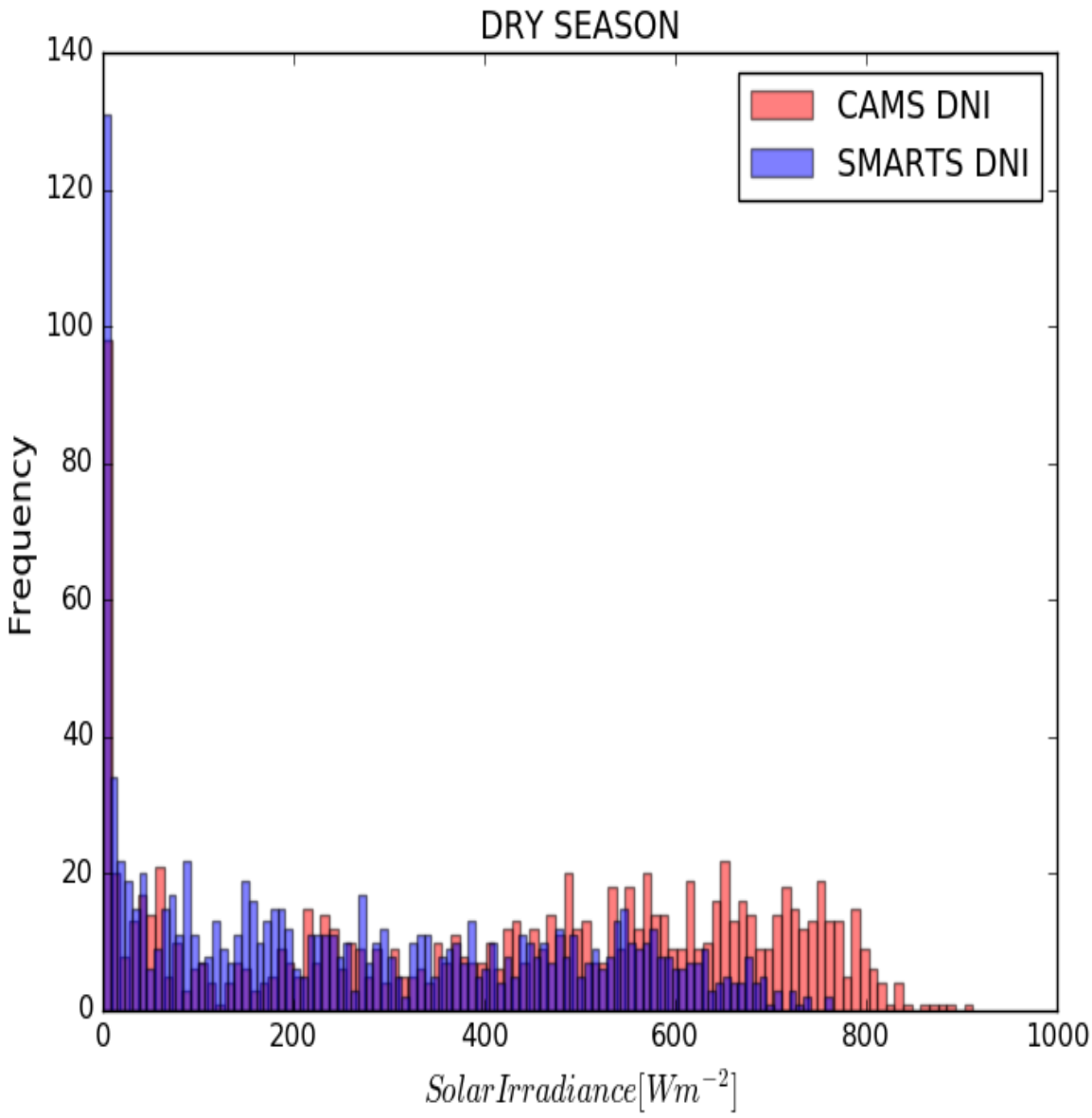

Figure 4.2: Histogram of dry season DNI

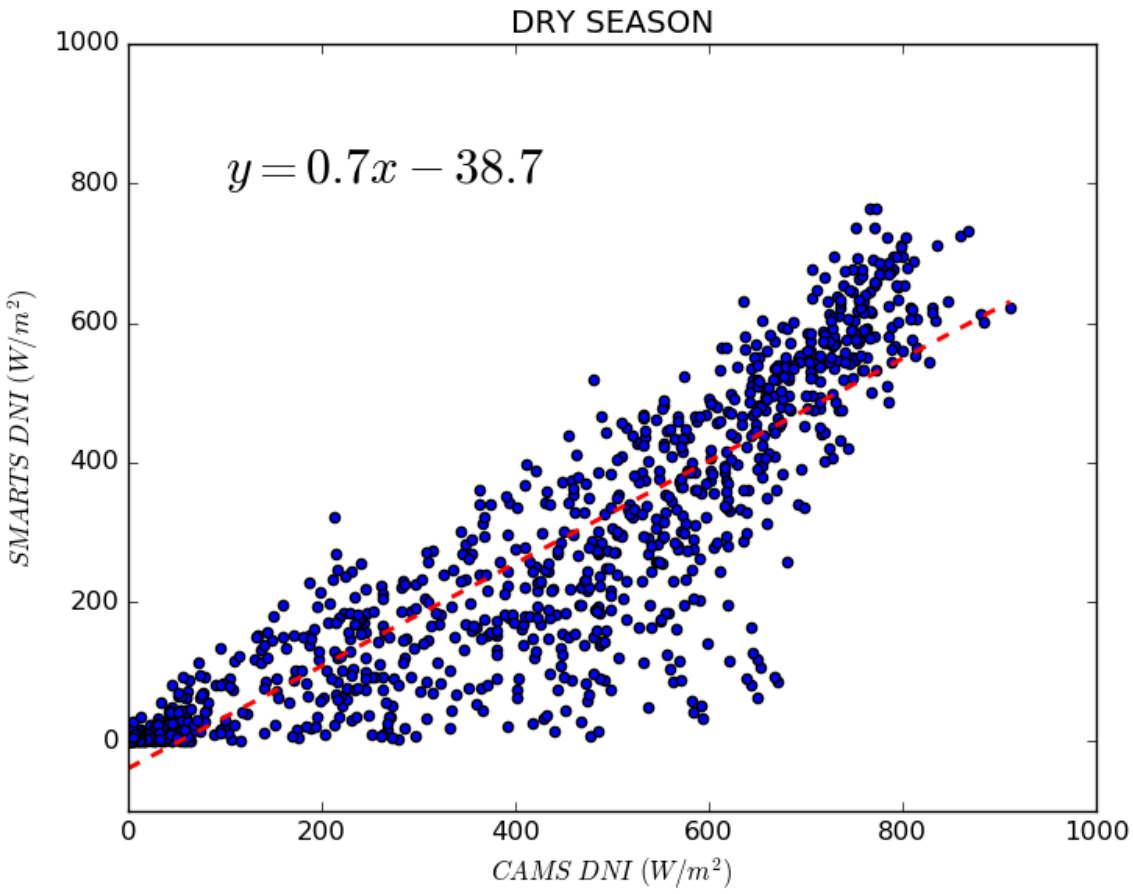

Figure 4.3: Scatterplot of dry season DNI

Table 4.1: Statistical data of dry season DNI

Data	**Mean**	**Standard Deviation**	**SE of Mean**	**Minimum (W/m^2)**	**Maximum (W/m^2)**
CAMS DNI	412.34783	263.17362	8.21215	0	911.8561
SMARTS DNI	264.12418	217.11689	6.77499	0	764.42406

Next, we look at the dry season Global Horizontal Irradiance (GHI) dry season plots below;

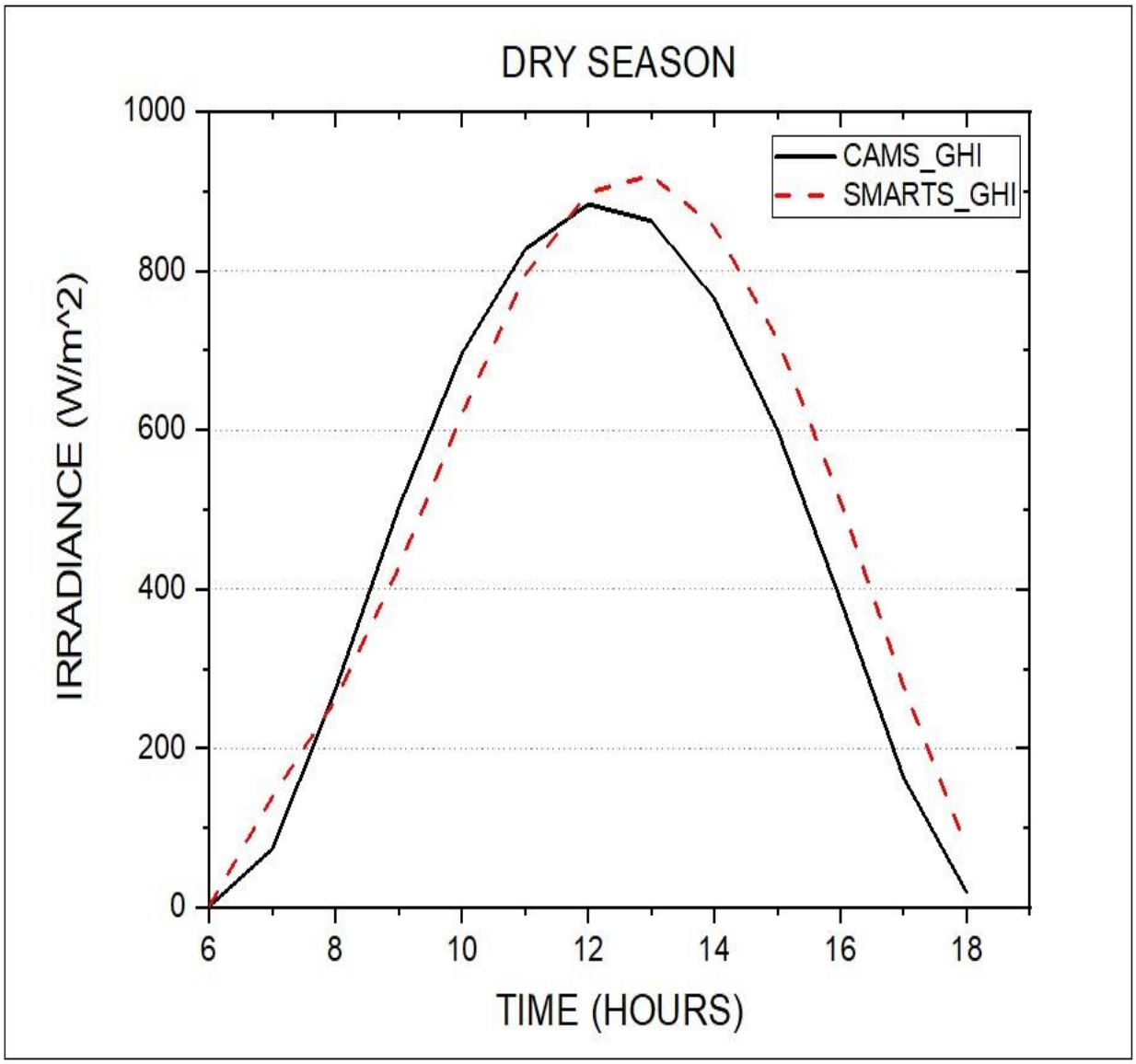

Figure 4.4: Hourly average global horizontal irradiance plot in the dry season

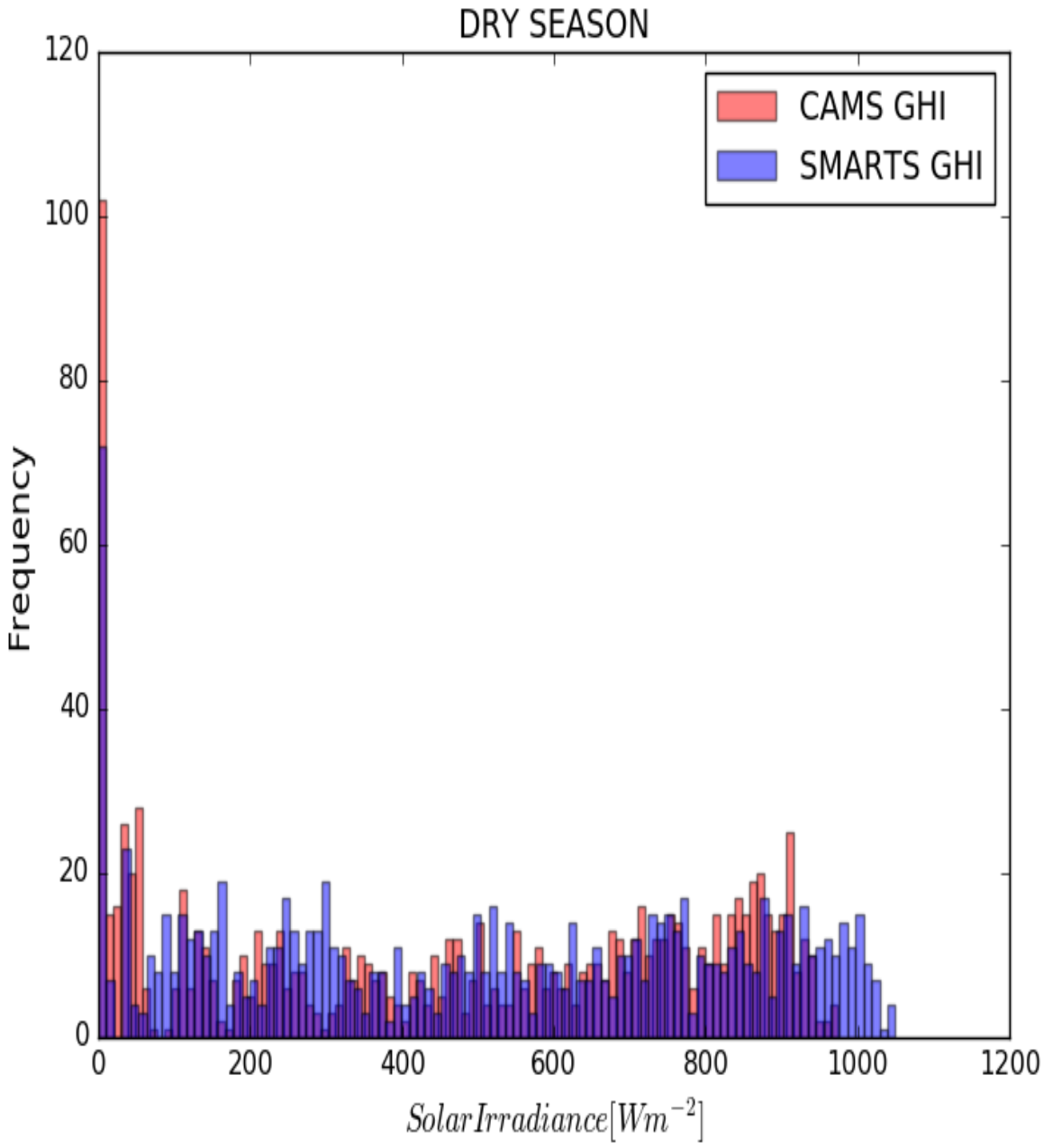

Figure 4.5: Histogram of dry season GHI

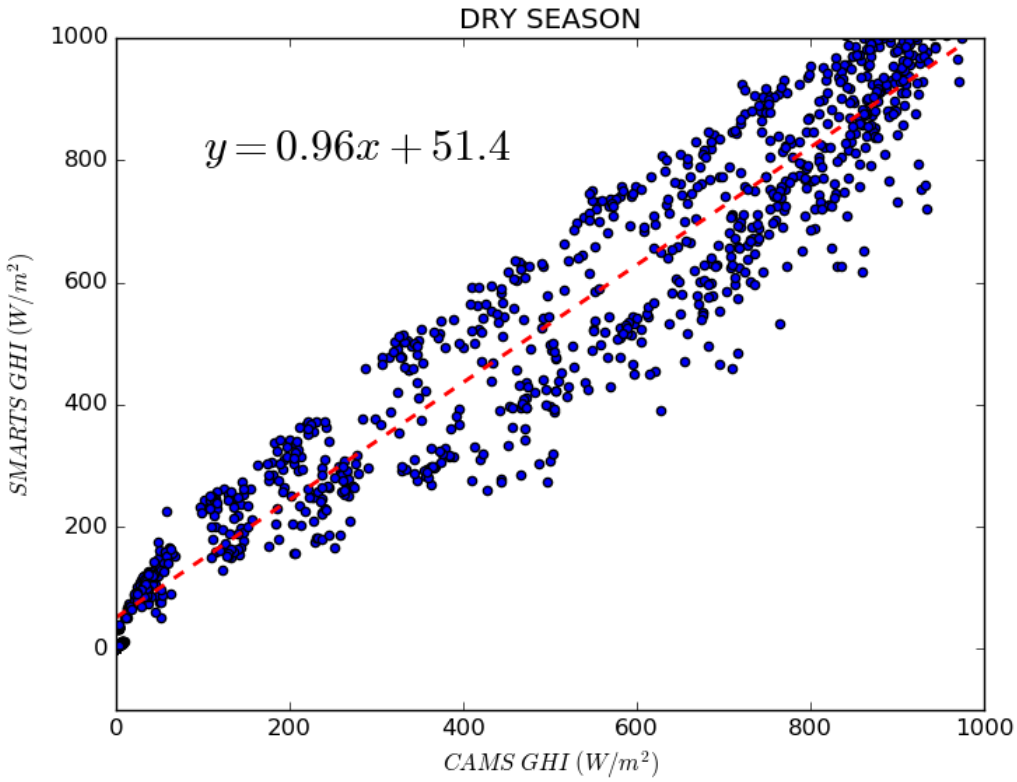

Figure 4.6: Scatterplot of dry season GHI

Table 4.2: Statistical data of dry season GHI

Data	Mean	Standard Deviation	SE of Mean	Minimum (W/m^2)	Maximum (W/m^2)
CAMS GHI	466.01633	324.19027	10.11614	0	973.7283
SMARTS GHI	499.75059	323.24978	10.08679	0	1049.7578

4.2 Rainy Season

The variation of shortwave solar irradiance during the wet season will be reviewed in this section. This season is characterized by precipitation (rain) and cloud cover, which results in a low clearness index (KT). The wet season begins from the month of April through to October in the study area. An average hourly value of irradiance was used for the plots shown below;

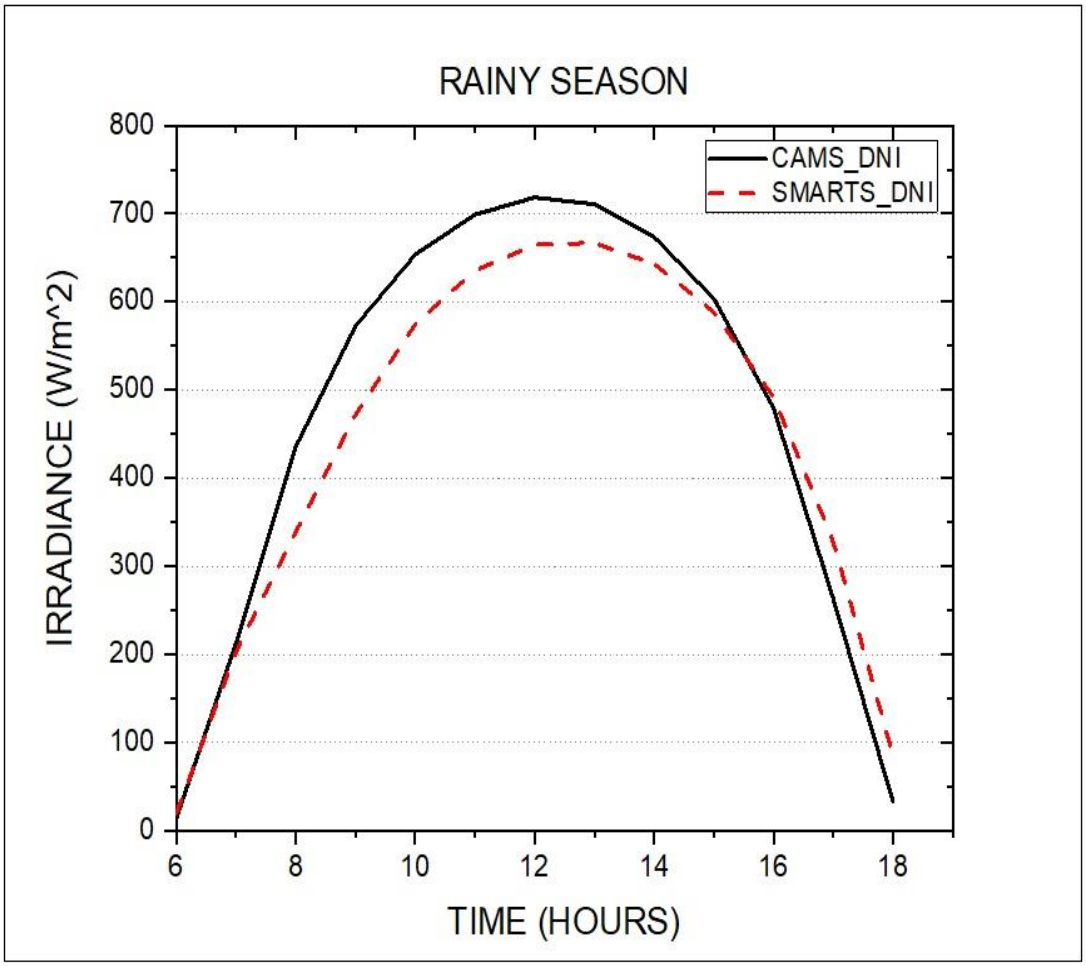

Figure 4.7: Hourly average direct normal irradiance plot in the rainy season

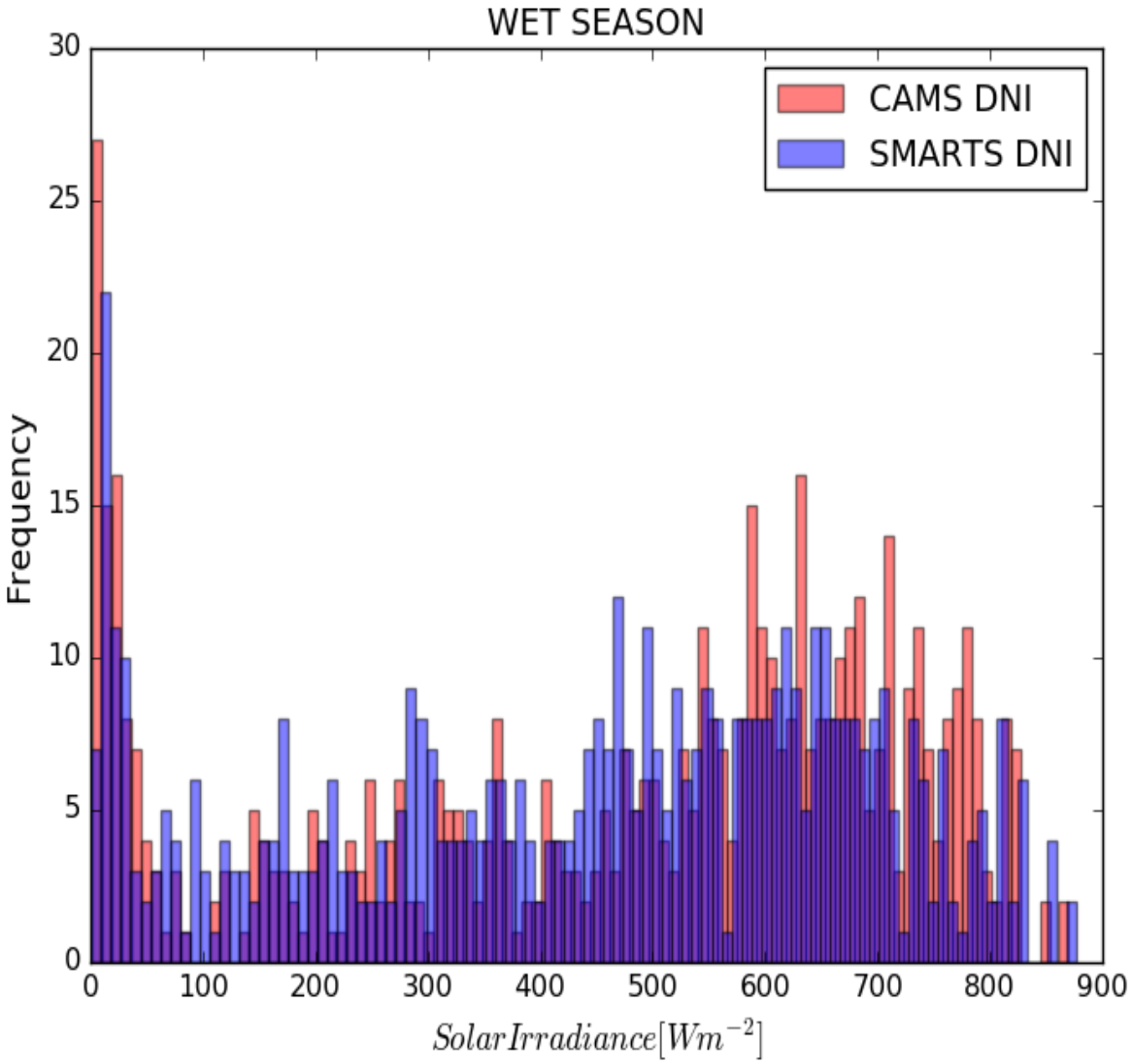

Figure 4.8: Histogram of rainy season DNI

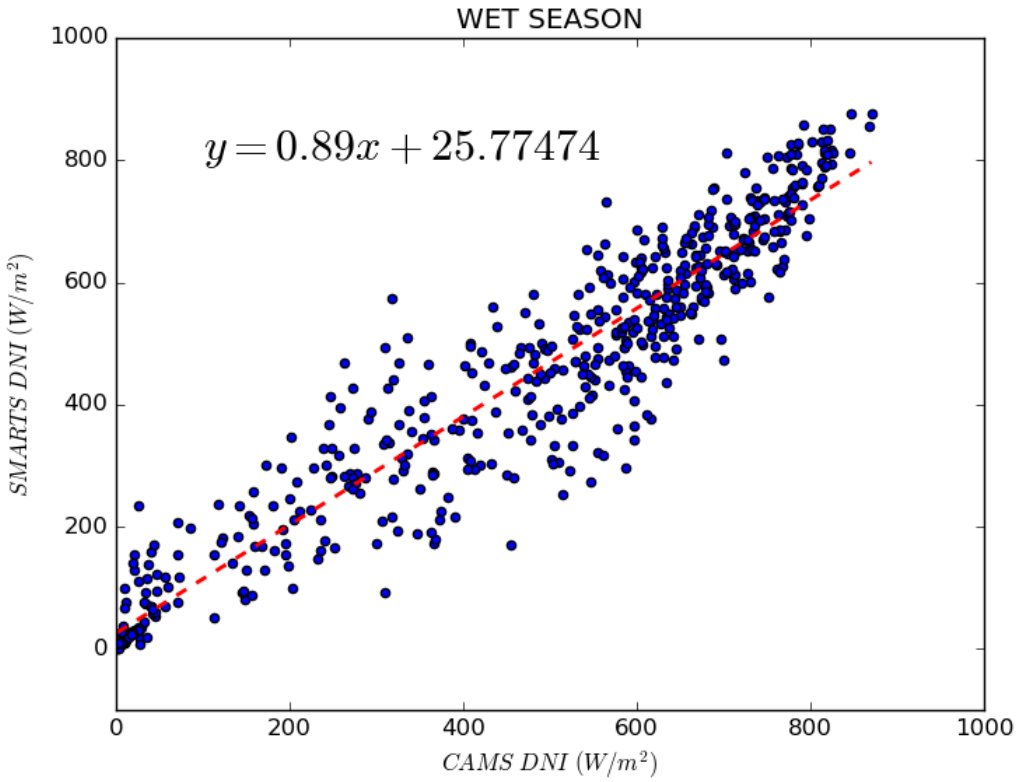

Figure 4.9: Scatterplot of rainy season DNI

Table 4.3: Statistical data of rainy season DNI

Data	Mean	Standard Deviation	SE of Mean	Minimum (W/m^2)	Maximum (W/m^2)
CAMS DNI	466.91847	257.82309	11.03381	1.2164	870.2179
SMARTS DNI	439.5419	240.93166	10.31092	0.5267	876.42949

Next, we look at the rainy season Global Horizontal Irradiance (GHI) plots;

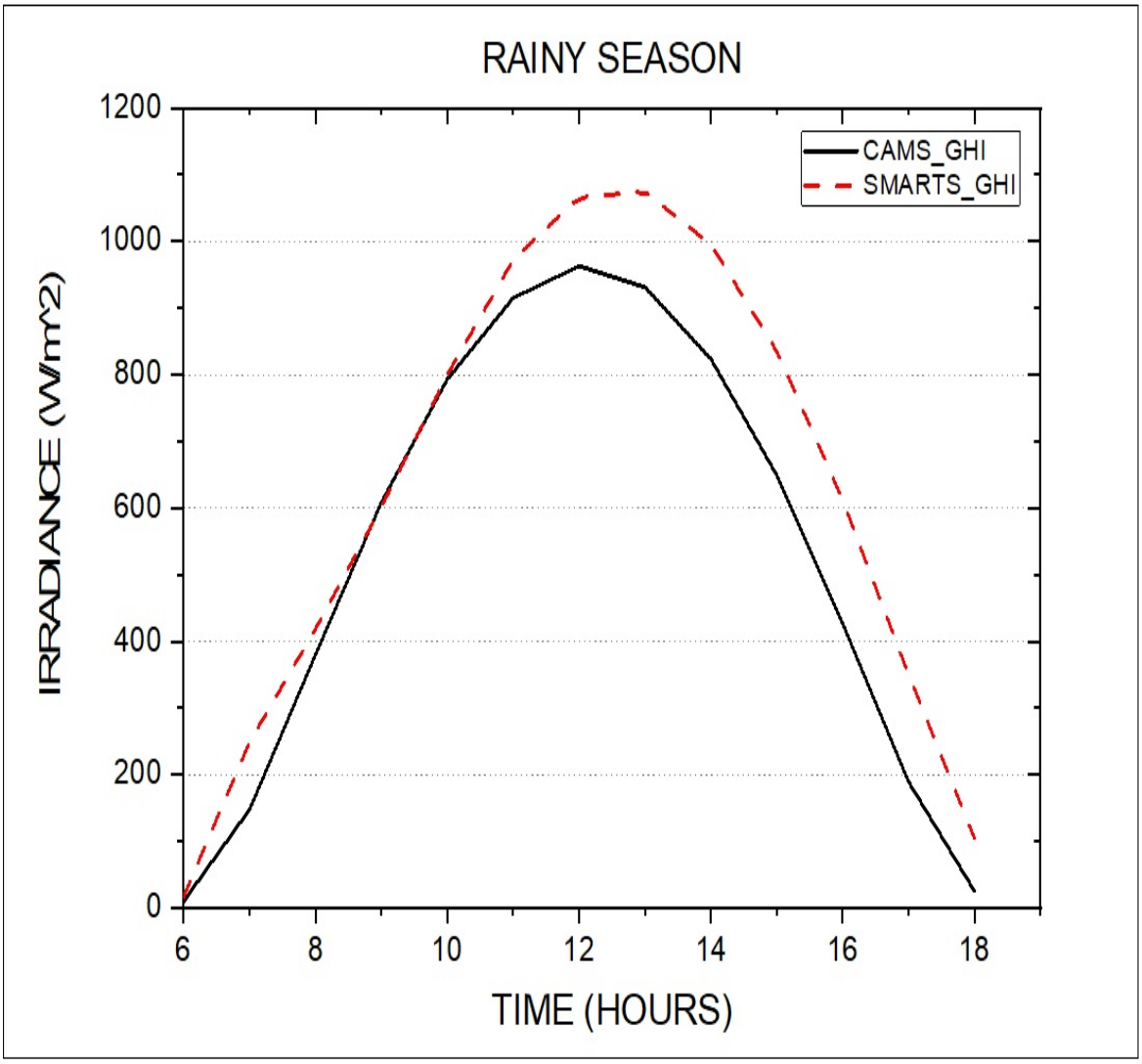

Figure 4.10: Hourly average global horizontal irradiance plot in the rainy season

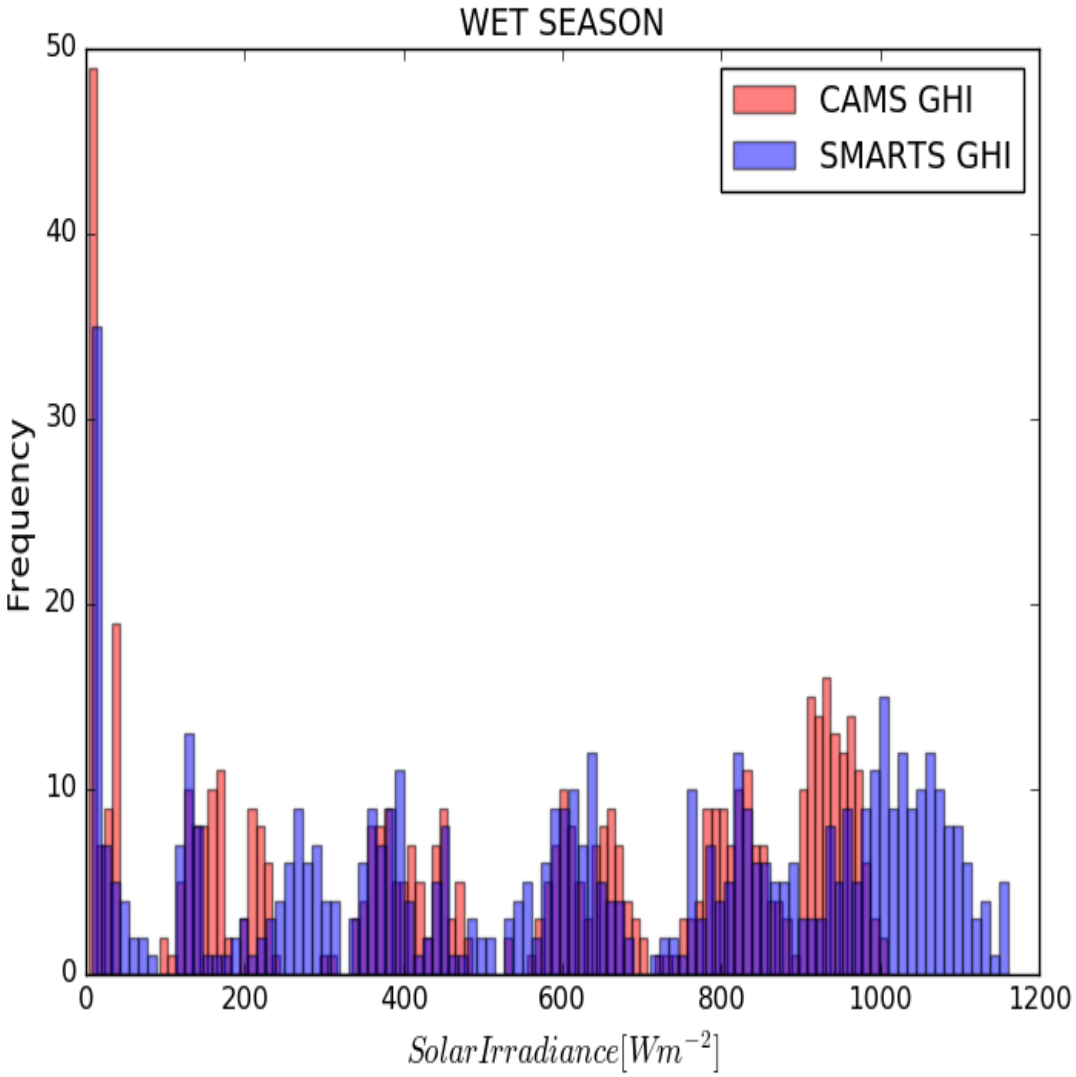

Figure 4.11: Histogram of rainy season GHI

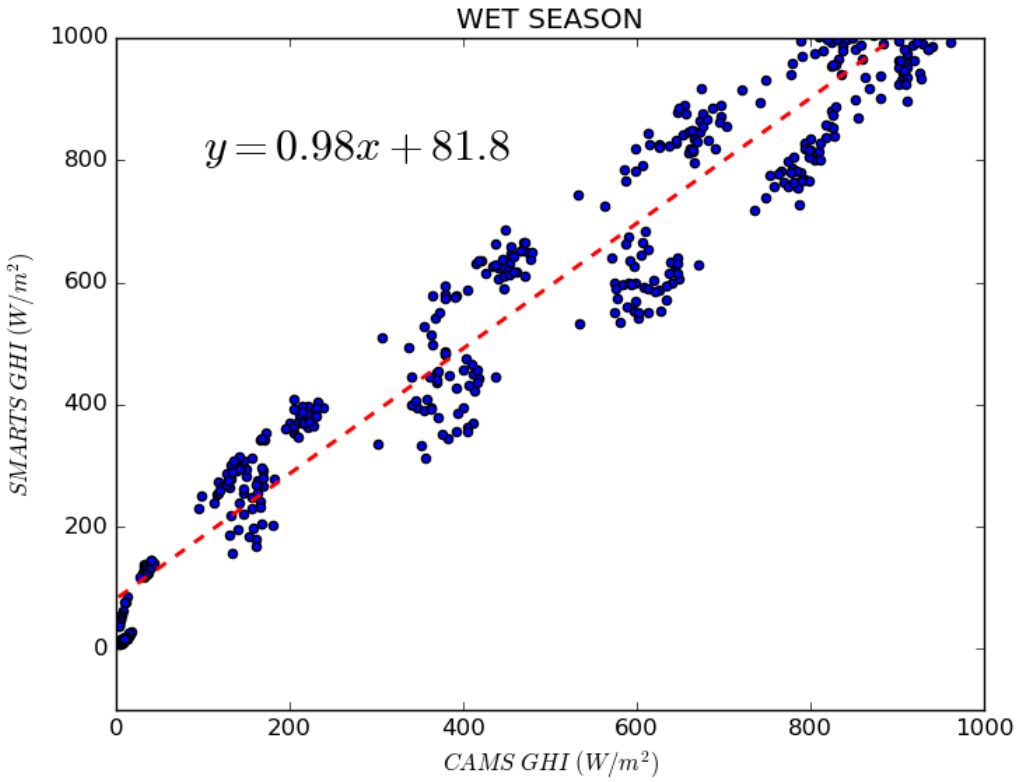

Figure 4.12: Scatterplot of rainy season GHI

Table 4.4: Statistical data of rainy season GHI

Data	Mean	Standard Deviation	SE of Mean	Minimum (W/m^2)	Maximum (W/m^2)
CAMS GHI	527.92721	340.27275	14.56233	2.9561	1008.0899
SMARTS GHI	622.8588	356.66963	15.26405	8.24785	1160.5703

4.3 Statistical Characterization of Differences in SMARTS Vs CAMS

In this subsection, we look at the SMARTS data characterization when compared to CAMS.

Table 4.5: Dry season statistical characterization

Data	Bias	Rel. **B**ias	RMS	Rel. RMS	RMSE
SMARTS DNI	148	0.56	191	0.46	171.77
SMARTS GHI	33.7	0.068	92	0.18	75.11

Table 4.6: Rainy season statistical characterization

Data	Bias	Rel. **B**ias	RMS	Rel. RMS	RMSE
SMARTS DNI	27	0.06	86	0.18	57.51
SMARTS GHI	95	0.18	121	0.18	116.73

4.4 Monthly Irradiance variation

In this section, the average monthly values of the irradiance over the year of study (2020) were compared with the Clearness Index (KT) in the plots shown below;

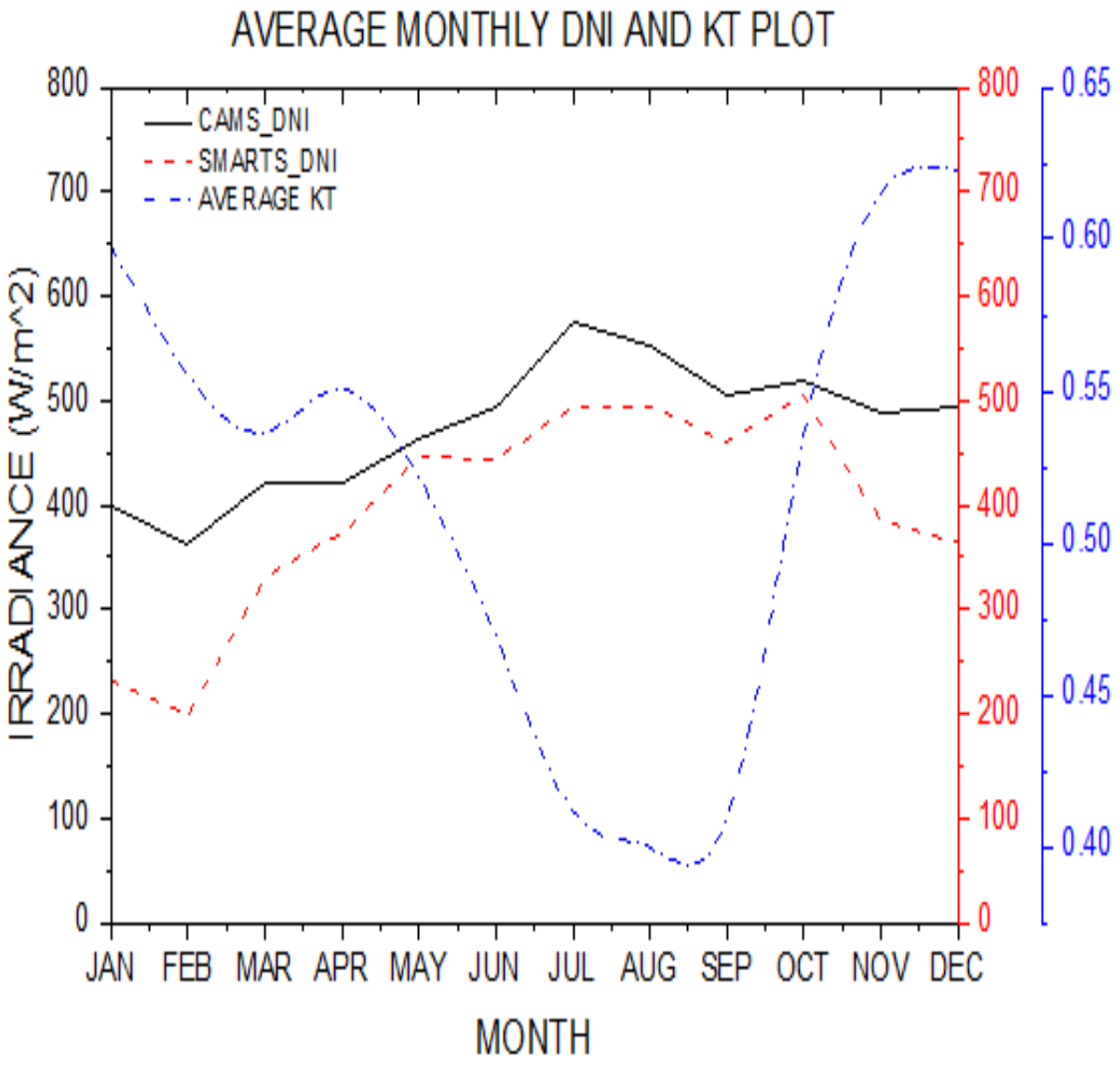

Figure 4.13: Average monthly direct normal irradiance and clearness index plot

The plot for the Global Horizontal Irradiance is shown below;

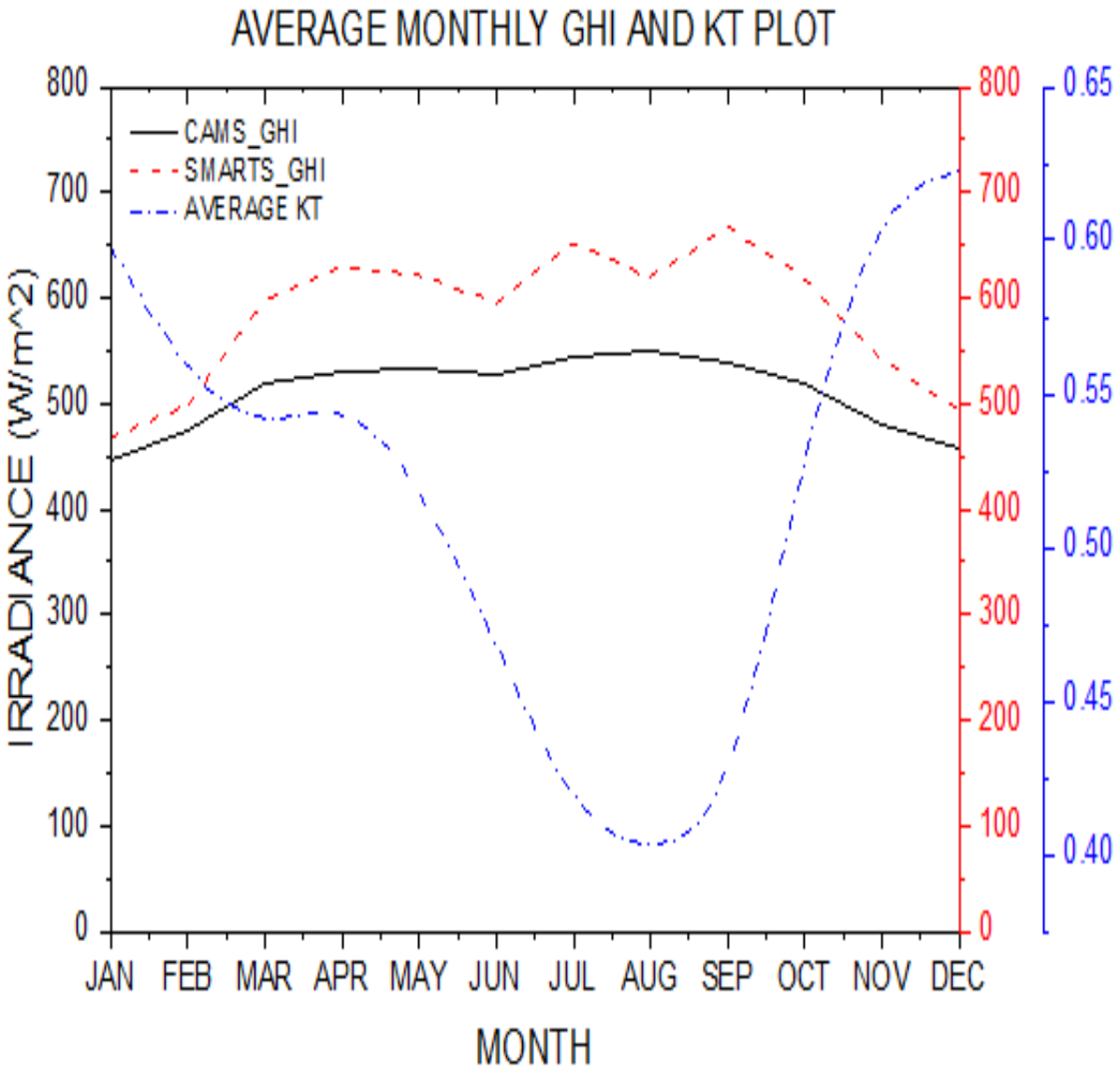

Figure 4.14: Average monthly global horizontal irradiance and clearness index plot

4.5 Discussion

In this section, we look at the results in the previous sections of this chapter;

4.5.1 Seasonal Variation of Irradiance

During the dry season, the difference is most glaring in comparison, with a higher margin for every parameter considered as shown in the table. The disparity between datasets is high although they follow a similar trend during the hours of this study. There is on average no Direct Normal Irradiance at 6.00 hours for both the model SMARTS and CAMS. The values are closer as sunset approaches in the evening. In this season, the model SMARTS has a maximum value of 764.42 W/m^2 and a minimum of 0. CAMS has the same minimum of 0 but a higher maximum of 911.8561 W/m^2.

In contrast to the Direct Normal Irradiance, the hourly average Global Horizontal Irradiance plot in the dry season shows a higher similarity between the model SMARTS and CAMS. The difference observed is a lag in the CAMS which peaks at 12.00 hours while SMARTS peaks at 13.00 hours. While both datasets have a minimum of 0, CAMS and SMARTS have a maximum of 973.7283 W/m^2 and 1049.7578 W/m^2 respectfully.

From the plot for the Direct Normal Irradiance in the rainy season, it is observed that both datasets are similar in value from dawn till about 8.00 hours after which CAMS is on average higher than SMARTS. They follow the same trend and are closer in value from about 15.00 hours. The model has a higher value at 18.00 hours on average implying the model has a later sunset time. Their minimums show a dawn time earlier than 6.00 hours, while CAMS and SMARTS have a maximum of 870.2179 W/m^2 and 876.42949 W/m^2 respectfully.

As seen in the rainy season plots of Global Horizontal Irradiance above, the modeled SMARTS irradiance is on average higher than the CAMS. There is an hour lag in their peaks as observed in the dry season as well. They follow the same trend and as seen in the DNI plot, SMARTS has a higher value at 18.00 hours, meaning a later sunset as well. Rainy season GHI values of the CAMS and SMARTS have a maximum of 1008.0899 W/m^2 and 1160.5703 W/m^2 respectfully.

The results show the highest disparity to be in the dry season for DNI irradiance, this is a result of the harmattan dust storms coming from the north. It is prevalent in the dry season at the study

location, and the dust particles have high reflectivity properties. The lag observed in the datasets can be attributed to the fact that the CAMS dataset is based on geostationary meteorological satellites at an altitude of about 35,000 km, while the SMARTS dataset was modeled using ground-based equipment, which is expected to receive irradiance later.

4.5.2 Monthly variation of Irradiance

From the DNI graph in the previous section, they follow the same trend all year round but the CAMS Direct Normal Irradiance is shown to be on average higher than that of SMARTS. The point where the Clearness Index (KT) intersects with DNI lines in the graph signifies the start of the rainy season. The plots show the DNI variation is affected by KT dips especially when it dips to the lowest value during the rainy season. This is a result of cloud cover in the rainy season affecting the line of sight between the Sun and the horizontal plane.

As for the Global Horizontal Irradiance (GHI), the modeled SMARTS irradiance is on average higher than CAMS throughout the year of study. The KT has does not have a significant effect on the GHI because it is a combination of Direct Normal Irradiance and Diffuse Horizontal Irradiance. In the rainy season with significantly high cloud cover and, hence, a lower KT value, the Diffuse Horizontal Irradiance increases in value as more irradiance is diffused by the clouds before reaching the ground.

CHAPTER FIVE

CONCLUSION AND RECOMMENDATIONS

5.1 Conclusion

A comparative analysis of ground and satellite-based methods of estimating the Direct Normal Irradiance (DNI) and Global Horizontal Irradiance (GHI) at the bottom of the atmosphere in Ilorin, Nigeria has been reported. Results from the study reveal that the modeled DNI and GHI data were closest to the reference satellite-based dataset during the rainy and dry season respectively. The disparities and errors are higher for the modeled DNI and GHI during the dry and rainy season respectively.

Root Mean Square Error (RMSE) values also support the above stated observation of of the modeled irradiance is seen to be lowest in the Dry GHI and wet DNI. It has been established that the CAMS dataset is best for estimating Wet DNI, Dry GHI, wet GHI, and dry DNI, in the order of lowest to highest error.

5.2 Recommendations

The SMARTS model proved efficient in this work, it is recommended to be used in irradiance studies of locations in Nigeria where aerosol characterization data can be gotten. We also recommend that the CAMS can be adopted for studies in regions without the aforementioned data.

References

Anmeng, Z., Enchao, L., Xin, L. and Xiaobing, Z.: Design and application of visible-near infrared band spectral radiation acquisition system, Journal of Applied Optics, 40, 557–562, 2019.

Anton, D. K.: Introductory Note to Intergovernmental Panel on Climate Change, Fourth Assessment Synopsis Report Summary for Policy Makers and the Bali Action Plan, SSRN Electronic Journal, 2008.

Apell, Jennifer N. and McNeill, K.: Updated and validated solar irradiance reference spectra for estimating environmental photodegradation rates, Environmental Science: Processes & Impacts, 21, 427–437, 2019.

Aschwanden, M. J.: Solar Stereoscopy and Tomography, Living Reviews in Solar Physics, 8, 2011.

Ångström, A.: Solar Constant, Sun-Spots and Solar Activity, The Astrophysical Journal, 55, 24, 1922.

Babatunde, E.: Some solar radiation ratios and their interpretations with regards to radiation transfer in the atmosphere, Nigeria Journal of Pure and Applied Physics, 4, 2006.

Badescu, V.: Verification of some very simple clear and cloudy sky models to evaluate global solar irradiance, Solar Energy, 61, 251–264, 1997.

Beck, H. E., Zimmermann, N. E., McVicar, T. R., Vergopolan, N., Berg, A. and Wood, E. F.: Publisher Correction: Present and future Köppen-Geiger climate classification maps at 1-km resolution, Scientific Data, 7, 2020.

Blanc, P., Espinar, B., Geuder, N., Gueymard, C., Meyer, R., Pitz-Paal, R., Reinhardt, B., Renné, D., Sengupta, M., Wald, L. and Wilbert, S.: Direct normal irradiance related definitions and applications: The circumsolar issue, Solar Energy, 110, 561–577, 2014.

Bolonkin, A. and Friedlander, J.: Explosion of Sun, Computational Water, Energy, and Environmental Engineering, 02, 83–96, 2013.

Borak, T. B. and Turner, J. E.: Atoms, Radiation, and Radiation Protection, Radiation Research, 146, 120, 1996.

Cachorro, V. E., Utrillas, M. P., Martinez-Lozano, J. A. and de Frutos, A. M.: A preliminary assessment of a detailed two stream short-wave narrow-band model using spectral radiation measurements, Solar Energy, 61, 265–273, 1997.

Charbonneau, P.: Dynamo Models of the Solar Cycle, Living Reviews in Solar Physics, 7, 2010.

ChemViews: The Electromagnetic Spectrum, ChemViews, 2015.

Chruścińska, A.: Influence of spectral width of stimulation band on the shape of OSL curve, Radiation Measurements, 56, 18–22, 2013.

Coddington, O., Lean, J. L., Pilewskie, P., Snow, M. and Lindholm, D.: A Solar Irradiance Climate Data Record, Bulletin of the American Meteorological Society, 97, 1265–1282, 2016.

Crisp, D.: Absorption of sunlight by water vapor in cloudy conditions: A partial explanation for the cloud absorption anomaly, Geophysical Research Letters, 24, 571–574, 1997.

Crommelynck, D., Fichot, A., Lee, R. B. and Romero, J.: First realisation of the Space Absolute Radiometric Reference (SARR) during the ATLAS 2 flight period, Advances in Space Research, 16, 17–23, 1995.

Darula, S., Kittler, R. and Gueymard, C. A.: Reference luminous solar constant and solar luminance for illuminance calculations, Solar Energy, 79, 559–565, 2005.

Dendy, R. O., Chapman, S. C. and Paczuski, M.: Fusion, space and solar plasmas as complex systems, Plasma Physics and Controlled Fusion, 49, 2007.

Du, Z. L.: Towards understanding the frequency distribution of solar flares—part 1: a Stochastic-Diffusive model of solar flares, Astrophysics and Space Science, 359, 2015.

Durney, B. R. and Spruit, H. C.: On the Dynamics of the Solar Convection Zone, International Astronomical Union Colloquium, 51, 15–16, 1980.

Feynman, R. P., Leighton, R. B., Sands, M. and Treiman, S. B.: The Feynman Lectures on Physics, Physics Today, 17, 45–46, 1964.

Forgács-Dajka, E.: Dynamics of the fast solar tachocline, Astronomy & Astrophysics, 413, 1143–1151, 2004.

García, O. E., Díaz, J. P., Expósito, F. J., Díaz, A. M., Dubovik, O., Derimian, Y., Dubuisson, P. and Roger, J.-C.: Shortwave radiative forcing and efficiency of key aerosol types using AERONET data, Atmospheric Chemistry and Physics, 12, 5129–5145, 2012.

Ghan, S. J., Smith, S. J., Wang, M., Zhang, K., Pringle, K., Carslaw, K., Pierce, J., Bauer, S. and Adams, P.: A simple model of global aerosol indirect effects, Journal of Geophysical Research: Atmospheres, 118, 6688–6707, 2013.

Gilgen, H., Wild, M. and Ohmura, A.: Means and Trends of Shortwave Irradiance at the Surface Estimated from Global Energy Balance Archive Data, Journal of Climate, 11, 2042–2061, 1998.

Glencross, W. M.: Role of plasma flow in determining structure of the chromosphere-corona transition zone of the sun, Solar Physics, 73, 1981.

Gombosi, T. I. and Holman, G. D.: Physics of the Space Environment, Physics Today, 52, 62–63, 1999.

Gueymard, C. A.: The sun's total and spectral irradiance for solar energy applications and solar radiation models, Solar Energy, 76, 423–453, 2004.

Gueymard, C. A.: Interdisciplinary applications of a versatile spectral solar irradiance model: A review, Energy, 30, 1551–1576, 2005.

Gueymard, C. A.: Direct and indirect uncertainties in the prediction of tilted irradiance for solar engineering applications, Solar Energy, 83, 432–444, 2009.

Gueymard, C. A.: Temporal variability in direct and global irradiance at various time scales as affected by aerosols, Solar Energy, 86, 3544–3553, 2012.

Gueymard, C. A.: The SMARTS spectral irradiance model after 25 years: New developments and validation of reference spectra, Solar Energy, 187, 233–253, 2019.

Gueymard, C. A. and Ruiz-Arias, J. A.: Validation of direct normal irradiance predictions under arid conditions: A review of radiative models and their turbidity-dependent performance, Renewable and Sustainable Energy Reviews, 45, 379–396, 2015.

Haigh, J. D.: The Sun and the Earth's Climate, Living Reviews in Solar Physics, 4, 2007.

Hotta, H. and Yokoyama, T.: Modeling Of Differential Rotation In Rapidly Rotating Solar-Type Stars, The Astrophysical Journal, 740, 12, 2011.

Howard, R.: Magnetic field rotation at high solar latitudes, Solar Physics, 59, 243–248, 1978.

Hughes, D. W. and Proctor, M. R. E.: Magnetic Fields in the Solar Convection Zone: Magnetoconvection and Magnetic Buoyancy, Annual Review of Fluid Mechanics, 20, 187–223, 1988.

Ineichen, P.: Validation of models that estimate the clear sky global and beam solar irradiance, Solar Energy, 132, 332–344, 2016.

Iorio, L.: An Empirical Explanation of the Anomalous Increases In The Astronomical Unit And The Lunar Eccentricity, The Astronomical Journal, 142, 68, 2011.

Janssen, K. and Cauzzi, G.: Dynamics of the solar photosphere with IBIS, Astronomy & Astrophysics, 450, 365–374, 2006.

Kaskaoutis, D. G. and Kambezidis, H. D.: The choice of the most appropriate aerosol model in a radiative transfer code, Solar Energy, 82, 1198–1208, 2008a.

Kaskaoutis, D. G. and Kambezidis, H. D.: The role of aerosol models of the SMARTS code in predicting the spectral direct-beam irradiance in an urban area, Renewable Energy, 33, 1532–1543, 2008b.

Kawamoto, K. and Hayasaka, T.: Relative contributions to surface shortwave irradiance over China: A new index of potential radiative forcing, Geophysical Research Letters, 35, 2008.

Kellner, L.: 4. The infra-red absorption of atmospheric gases, Quarterly Journal of the Royal Meteorological Society, 68, 204–205, 1942.

Kohn, H. I.: Sources, Effects and Risks of Ionizing Radiation, Radiation Research, 120, 187, 1989.

Kopp, G. and Lean, J. L.: A new, lower value of total solar irradiance: Evidence and climate significance, Geophysical Research Letters, 38, 2011.

Korsós, M.: Predicting CMEs And Solar Flares, Science Trends, 2018.

Koskinen, H.: Physics of the upper polar atmosphere by Askeir Brekke, Planetary and Space Science, 46, 343, 1998.

Lawin, A. E., Niyongendako, M. and Manirakiza, C.: Solar Irradiance and Temperature Variability and Projected Trends Analysis in Burundi, Climate, 7, 83, 2019.

Lean, J.: Sun-Climate Connections: Earth's Response to a Variable Sun, Science, 292, 234–236, 2001.

Leavenworth, F. P.: Observation of the eclipse of the sun, NOV. 22, 1919, The Astronomical Journal, 32, 165, 1920.

Lohmann, U. and Feichter, J.: Global indirect aerosol effects: a review, Atmospheric Chemistry and Physics, 5, 715–737, 2005.

Maloney, E. D. and Shaman, J.: Intraseasonal Variability of the West African Monsoon and Atlantic ITCZ, Journal of Climate, 21, 2898–2918, 2008.

Michalsky, J., Dutton, E., Rubes, M., Nelson, D., Stoffel, T., Wesley, M., Splitt, M. and DeLuisi, J.: Optimal Measurement of Surface Shortwave Irradiance Using Current Instrumentation, Journal of Atmospheric and Oceanic Technology, 16, 55–69, 1999.

Míguez, H.: Sunlight Absorption Engineering for Thermophotovoltaics: Contributions from the Optical Design, ChemSusChem, 8, 786–788, 2015.

N'Datchoh, E. T., Diallo, I., Konaré, A., Silué, S., Ogunjobi, K. O., Diedhiou, A. and Doumbia, M.: Dust induced changes on the West African summer monsoon features, International Journal of Climatology, 38, 452–466, 2017.

Nandy, D.: Magnetic helicity and flux tube dynamics in the solar convection zone: Comparisons between observation and theory, Journal of Geophysical Research, 111, 2006.

Ossendrijver, M.: The solar dynamo, Astronomy and Astrophysics Review, 11, 287–367, 2003.

Ovechkin, G. V., Sandrigailo, L. E. and Bakhtovarshoev, Sh.: Some inferences on the properties of the radiation intensity growth curve of a spectral line, Journal of Applied Spectroscopy, 12, 23–28, 1970.

Pace, G., di Sarra, A., Meloni, D., Piacentino, S. and Chamard, P.: Aerosol optical properties at Lampedusa (Central Mediterranean). 1. Influence of transport and identification of different aerosol types, Atmospheric Chemistry and Physics, 6, 697–713, 2006.

Parfrey, K. P. and Menou, K.: The Origin of Solar Activity in the Tachocline, The Astrophysical Journal, 667, 2007.

Pinker, R. T., Frouin, R. and Li, Z.: A review of satellite methods to derive surface shortwave irradiance, Remote Sensing of Environment, 51, 108–124, 1995.

Pinker, R. T., Liu, H., Osborne, S. R. and Akoshile, C.: Radiative effects of aerosols in sub-Sahel Africa: Dust and biomass burning, Journal of Geophysical Research, 115, 2010.

Reno, M. J. and Hansen, C. W.: Identification of periods of clear sky irradiance in time series of GHI measurements, Renewable Energy, 90, 520–531, 2016.

Rodger, A.: Physics of the upper polar atmosphere, Journal of Atmospheric and Solar-Terrestrial Physics, 60, 404, 1998.

Rudraiah, N. and Venkatachalappa, M.: Propagation of internal gravity waves in perfectly conducting fluids with shear flow, rotation and transverse magnetic field, Journal of Fluid Mechanics, 52, 193–206, 1972.

Sage, C.: The similar effects of low-dose ionizing radiation and non-ionizing radiation from background environmental levels of exposure, The Environmentalist, 32, 144–156, 2012.

Sandorfy, C.: U.V. absorption of fluorocarbons, Atmospheric Environment (1967), 10, 343–351, 1976.

Seidel, F. C., Kokhanovsky, A. A. and Schaepman, M. E.: Fast and simple model for atmospheric radiative transfer, Atmospheric Measurement Techniques, 3, 1129–1141, 2010.

Small, J. D., Jiang, J. H., Su, H. and Zhai, C.: Relationship between aerosol and cloud fraction over Australia, Geophysical Research Letters, 38, 2011.

Tolento, J. P. and Robinson, T. D.: A simple model for radiative and convective fluxes in planetary atmospheres, Icarus, 329, 34–45, 2019.

Vuilleumier, L., Hauser, M., Félix, C., Vignola, F., Blanc, P., Kazantzidis, A. and Calpini, B.: Accuracy of ground surface broadband shortwave radiation monitoring, Journal of Geophysical Research: Atmospheres, 119, 2014.

Wagner, A., Bennouna, Y., Blechschmidt, A.-M., Brasseur, G., Chabrillat, S., Christophe, Y., Errera, Q., Eskes, H., Flemming, J., Hansen, K. M., Inness, A., Kapsomenakis, J., Langerock, B., Richter, A., Sudarchikova, N., Thouret, V. and Zerefos, C.: Comprehensive evaluation of the Copernicus Atmosphere Monitoring Service (CAMS) reanalysis against independent observations, Elementa: Science of the Anthropocene, 9, 2021.

Wandji Nyamsi, W., Blanc, P., Dumortier, D., Mouangue, R., Arola, A. and Wald, L.: Using Copernicus Atmosphere Monitoring Service (CAMS) Products to Assess Illuminances at Ground Level under Cloudless Conditions, Atmosphere, 12, 643, 2021.

Wielicki, B. A., Barkstrom, B. R., Harrison, E. F., Lee, R. B., Louis Smith, G. and Cooper, J. E.: Clouds and the Earth's Radiant Energy System (CERES): An Earth Observing System Experiment, Bulletin of the American Meteorological Society, 77, 853–868, 1996.

Wielicki, B. A., Barkstrom, B. R., Baum, B. A., Charlock, T. P., Green, R. N., Kratz, D. P., Lee, R. B., Minnis, P., Smith, G. L., Takmeng Wong, Young, D. F., Cess, R. D., Coakley, J. A., Crommelynck, D. A. H., Donner, L., Kandel, R., King, M. D., Miller, A. J., Ramanathan, V., Randall, D. A., Stowe, L. L. and Welch, R. M.: Clouds and the Earth's Radiant Energy System (CERES): algorithm overview, IEEE Transactions on Geoscience and Remote Sensing, 36, 1127–1141, 1998.

Woolfson, M.: The origin and evolution of the solar system, Astronomy & Geophysics, 41, 2000.

Xiao, G., Guo, K., Xu, W., Ni, M., Luo, Z. and Cen, K.: An improved method of Lambertian CCD-camera radiation flux measurement based on SMARTS (simple model of the atmospheric radiative transfer of sunshine) to reduce spectral errors, Energy, 67, 74–80, 2014.

Yusuf, N., Said S, R., Tilmes, S. and Gbobaniyi, E.: Multi-year analysis of aerosol optical properties at various timescales using AERONET data in tropical West Africa, Journal of Aerosol Science, 151, 105625, 2021.